HHS Public Access

Author manuscript

Nat Immunol. Author manuscript; available in PMC 2018 September 21.

Published in final edited form as:

Nat Immunol. 2018 April ; 19(4): 354–365. doi:10.1038/s41590-018-0071-9.

IL-17 receptor-associated adaptor Act1 directly stabilizes mRNAs to mediate IL-17 inflammatory signaling

Tomasz Herjan[#1,7], **Lingzi Hong**[#1], **Jodi Bubenik**[2], **Katarzyna Bulek**[1,8], **Wen Qian**[1], **Caini Liu**[1], **Xiao Li**[3], **Xing Chen**[1], **Hui Yang**[1], **Suidong Ouyang**[1], **Hao Zhou**[1], **Junjie Zhao**[1], **Vasu Komireddy**[2], **Eric Cockman**[2], **Mark Aronica**[6], **Kewal Asosingh**[6], **Donny D. Licatalosi**[4], **Jun Qin**[5], **Paul L. Fox**[2], **Thomas A. Hamilton**[1], **Donna Driscoll**[2], and **Xiaoxia Li**[1,10]

[1]Department of Immunology, Lerner Research Institute, Cleveland Clinic Foundation, Cleveland, Ohio, USA [2]Department of Cellular and Molecular Medicine, Lerner Research Institute, Cleveland Clinic Foundation, Cleveland, Ohio, USA [3]Department of Genetics, Stanford University School of Medicine, Stanford, CA, USA [4]Center for RNA Molecular Biology, Department of Biochemistry, Case Comprehensive Cancer Center, Case Western Reserve University, Cleveland, Ohio, USA [5]Department of Molecular Cardiology, Lerner Research Institute, Cleveland Clinic Foundation, Cleveland, Ohio, USA [6]Department of Pathobiology, Lerner Research Institute, Cleveland Clinic, Cleveland, OH 44195, USA [7]Department of General Biochemistry, Faculty of Biochemistry, Biophysics and Biotechnology, Jagiellonian University, Krakow 30-387, Poland [8]Department of Immunology, Faculty of Biochemistry, Biophysics, and Biotechnology, Jagiellonian University, Krakow 30-387, Poland

[#] These authors contributed equally to this work.

Abstract

Mechanisms that degrade inflammatory mRNAs are well-known, however stabilizing mechanisms are poorly understood. Here we show that Act1, an interleukin-17 (IL-17) receptor complex adaptor, binds and stabilizes mRNAs encoding key inflammatory proteins. The Act1 SEFIR domain binds a stem-loop structure, SBE (SEFIR-binding element), in the inflammatory chemokine *Cxcl1* 3' UTR. mRNA-bound Act1 directs formation of three compartmentally-distinct protein-RNA complexes (RNPs) that regulate three disparate events in inflammatory mRNA metabolism: preventing mRNA decay in the nucleus, inhibiting mRNA decapping in P-bodies, and

[10]Corresponding authors: Xiaoxia Li, Department of Immunology, Lerner Research Institute, Cleveland Clinic Foundation, Cleveland, OH, USA; lix@ccf.org.

Author contributions

T.H. and L.H. designed experiments, performed experiments, analyzed data and wrote the manuscript with input from the co-authors. J. B., K.B., W. Q., C. L., Xiao. L., X. C., H. Y., S. O., H. Z., J. Z., V. K. and E. C. assisted with experiments and participated in discussion.

M. A., K. A., D. D. L., J. Q., P. L. F., T. A. H. facilitated the experimentation and offered critical scientific discussion.

Xiaoxia. L. and D. D. designed experiments, analyzed data and wrote the manuscript with input from the co-authors.

Competing interests

The authors declare no competing financial interests.

Data availability statement

The primary data for analysis of all figures and supplementary figures are available upon request.

promoting translation. SBE RNA aptamers reduced IL-17-mediated mRNA stabilization *in vitro,* IL-17-induced skin inflammation and airway inflammation in a mouse asthma model, providing a therapeutic strategy for autoimmune diseases. These results reveal a network in which Act1 assembles RNPs on the 3' UTRs of select mRNAs to control receptor-mediated mRNA stabilization and translation during inflammation.

INTRODUCTION

Interleukin 17 (IL-17, also known as IL-17A) is a key signature cytokine of T_H17 cells and is also produced by innate immune cells[1, 2, 3]. IL-17A plays a critical role in the pathogenesis of autoimmune and inflammatory diseases, including psoriasis, rheumatoid arthritis, multiple sclerosis, and asthma[4, 5, 6].

IL-17A signals through a heterodimeric receptor complex (IL-17R) composed of IL-17RA and IL-17RC[7, 8]. Both IL-17RA and IL-17RC belong to a SEFIR protein family, which is defined by the presence of a conserved cytoplasmic SEFIR domain[9]. Act1 (encoded by the gene *TRAF3IP2,* also known as *CIKS*) is an essential component in IL-17 signaling and also a member of the SEFIR protein family[10, 11, 12]. Upon IL-17 stimulation, Act1 is recruited to IL-17R through a SEFIR-dependent interaction. Act1 in turn engages members of the TRAF family, activating NF-kB, C/EBP, and MAPK pathways. IL-17-Act1-mediated signaling results in transcription of pro-inflammatory and neutrophil-mobilizing cytokines and chemokines, including *Cxcl1*, *Tnf*, *Il-6* and *Csf2*[13].

While IL-17 activates gene transcription of cytokines and chemokines, it is equally important for IL-17 to stabilize otherwise unstable mRNAs for the induction of the proinflammatory genes. Cytokine and chemokine mRNAs have short half-lives because of conserved cis-elements, including AU-rich elements (AREs) and stem-loop structures in their 3' UTRs[14, 15]. The AREs within the 3' UTRs can be recognized by RNA binding proteins (including TTP, AUF1, KSRP and SF2) that function to mediate the sequential deadenylation, decapping, and ultimately exonucleolytic degradation of the RNA[16, 17]. Stem-loops are present in immune-related mRNAs (including *Tnf* and *Il6*), and are destabilized by the RNA binding proteins Roquin and Regnase-1. Stress granules form in response to stress, store mRNAs stalled in translation and transfer them to Processing-bodies (P-bodies) for degradation. Roquin destabilizes translationally inactive mRNAs that are accumulated in P-bodies and stress granules whereas Regnase-1 specifically cleaves and degrades translationally active mRNAs bound to polysomes[18]. While multiple mRNA destabilizing mechanisms have been discovered, little is understood about the stabilization of mRNAs encoding inflammatory factors. Although ARE binding protein SF2 (Splicing factor 2) and HuR (human antigen R) were previously implicated in IL-17-induced mRNA stabilization, the recruitment of SF2 and HuR cannot explain the receptor-specific mRNA stabilization of select inflammatory genes[19, 20].

Here we demonstrate that Act1 behaves as an RNA-binding protein that interacts with the stem-loop structure of select inflammatory mRNAs such as *Cxcl1*, *Tnf* and *Csf2*. Act1-binding results in stabilization of the mRNA and thereby mediates the proinflmmatory effects of IL-17 signaling. RNA aptamers containing the stem-loop structure (referred to

here as SBE), inhibited Act1's binding to target mRNAs and attenuated IL-17-mediated mRNA stabilization and reduced pathology in mouse models of asthma and skin inflammation. This data provides the first example of a receptor-interacting adaptor molecule, Act1, playing a direct role in mRNA metabolism, and elucidates a new mechanism for receptor-mediated selectivity of mRNA stabilization and translation. This mechanistic understanding of the action of Act1 might yield novel therapeutic strategies for treating inflammatory diseases.

RESULTS

IL-17 induces distinct Act1-RNPs in the nucleus and cytoplasmic granules

Messenger RNAs that are not engaged in translation can aggregate into cytoplasmic mRNP granules referred to as P-bodies and stress granules[21, 22]. IL-17A stimulation induced the assembly of Act1, the key adaptor of IL-17R, into microscopically visible cytoplasmic granules and nuclear localization (Fig. 1a and [23]). Act1 was co-localized with Dcp1 decapping enzyme, a component of P-bodies (Fig. 1b); but not with TIA1 (a marker for stress granules) or IRAK1 (IL-1R associated kinase 1) (Fig. 1b). To investigate IL-17A-induced interaction of endogenous Act1 with Dcp1, we generated LSL–HA–Act1 knock-in mice by knocking a LoxP-Stop-LoxP-Traf3ip2 cDNA-HA-Tag PolyA cassette into the endogenous Act1 locus (Supplementary Fig. 1a and Material and Methods). Using mouse embryonic fibroblasts (MEFs) isolated from the UBC-Cre-ERT2/LSL-HA-Act1$^{f/+}$ mice, we detected the interaction between the endogenous HA-Act1 and Dcp1 in response to IL-17A stimulation by in situ Proximity Ligation Assay (Supplementary Fig. 1b) and co-immunoprecipitation (Fig. 1c). RNase pretreatment of the lysates abolished the Act1-Dcp1 interaction (Fig. 1c), implicating the possible role of IL-17-Act1 axis in mRNA metabolism in the P-bodies.

In addition to Act1-Dcp1 interaction, IL-17A induced interaction of HA-Act1 with SF2 and HuR in the nucleus and cytoplasmic granules, respectively (Supplementary Fig. 1c and [20]). However, IL-17A stimulation failed to induce visible interaction of Dcp1 with SF2 and HuR either in the nucleus or cytoplasm (Supplementary Fig. 1c-f). These results indicate that Act1's interaction with Dcp1 in the P-bodies is likely independent from the Act1-SF2 and Act1-HuR complexes. Notably, RNase pretreatment of the lysates abolished the Act1-SF2 and Act1-HuR interaction (Fig. 1c and Supplementary Fig. 1d-f). Taken together, these results implicate the IL-17-Act1 axis in mRNA metabolism via formation of distinct Act1-containing RNPs, including Act1-SF2 (RNP1), Act1-Dcp1 (RNP2) and Act1-HuR (RNP3). As controls, we showed that while IL-17E (also known as IL-25, another member of IL-17 family) also induced the formation of Act1-RNPs (interaction with SF2, Dcp1 or HuR), IL-1 stimulation failed to induce the formation of Act1-RNPs (interaction with SF2, Dcp1 or HuR) (data not shown).

The SEFIR domain of Act1 is required for the formation of Act1-RNPs

Deletion analysis showed the SEIFR domain of Act1 was necessary and sufficient for Act1 to assemble into granules and co-localize with Dcp1 (Fig. 1d and Supplementary Fig. 1g). Although SEFIR3 (463–501 aa) of Act1 is required for its interaction with IL-17R[24],

ΔSEFIR3 was still localized to the P-bodies (Fig. 1d and Supplementary Fig. 1g). While ΔSEFIR5 showed reduced co-localization with P-bodies, ΔSEFIR1 completely failed to reside in the P-bodies (Fig. 1d and Supplementary Fig. 1g). ΔSEFIR1 also failed to interact with Dcp1, SF2 and HuR in the co-immunoprecipitation experiment (Fig. 1e). On the other hand, both ΔSEFIR1 and ΔSEFIR5 retained their ability to interact with IL-17R (data not shown). Taken together, these results indicate that the SEFIR domain of Act1 is required for the formation of Act1-RNPs.

Act1 directly binds to the *Cxcl1* 3' UTR through the SEFIR domain

We then modeled the SEFIR domain of Act1 by SWISS-Model(http://swissmodel.expasy.org), using the crystal structure of IL-17RA-SEFIR as a template. Helix αA from SEFIR1 and helix αE from SEFIR5 are located in close proximity in Act1 SEFIR domain forming a positively charged surface (Fig. 2a). The corresponding helix αA and helix αE from IL-17RA are not located on the same surface and the helix αE is negatively charged (Fig. 2a). The SEFIR1+SEFIR5 positively charged surface in Act1 might provide an interaction interface with negatively charged mRNAs. To test such a possibility, we subjected Act1 SEFIR and IL-17RA SEFIR to RNA electrophoretic mobility shift assay (REMSA) on *Cxcl1* 3'UTR, which was shown to be regulated by the IL-17-Act1-axis for stabilization of *Cxcl1* mRNA[25, 26]. Recombinant Act1 SEFIR, but not IL-17RA SEFIR, bound to the *Cxcl1* probe with Kd=50.2±7.8 nM (Fig. 2b and Supplementary Fig. 2a). Act1 SEFIR failed to bind the GC-rich 3' UTR of Glutathione Peroxidase 4 (GPx4) (Fig. 2b). While ΔSEFIR2, ΔSEFIR3 and ΔSEFIR4 retained the ability to bind RNA, ΔSEFIR1 and ΔSEFIR5 had much reduced binding to RNA (Supplementary Fig. 2b-f). Mutation of the positively charged amino acid residues in SEFIR1 (K407A) or SEFIR5 (K524A/K526A/K527A) substantially reduced the binding of Act1 SEFIR to RNA, whereas SEFIR1+5mt (K407A/K524A/K526A/K527A) abolished the RNA binding (Fig. 2c), supporting the proposed RNA interaction interface of Act1 SEFIR in Fig. 2a. The impaired RNA binding of Act1 mutants (ΔSEFIR1 and SEFIR1+5mt) correlated with their inability to enter the P-bodies (Fig. 1d and Supplementary Fig. 1g) and form the RNPs (Fig. 1e and Supplementary Fig. 1d-f), which is consistent with the RNA-dependent Act1's interaction with Dcp1, SF2 and HuR shown in Fig. 1c.

Act1 mediates mRNA stabilization of *Cxcl1*, *Csf2* and *Tnf* via direct binding to their 3' UTRs

We then tested Act1 mutants of ΔSEFIR1 and SEFIR1+5mt (that lost RNA binding) for their ability to restore IL-17 signaling and gene expression in Act1-deficient MEFs. Act1 mutants of ΔSEFIR1 and SEFIR1+5mt still retained their interaction with the IL-17R (Fig. 2d and supplementary Fig. 3a) and were able to mediate IL-17A-induced NFkB, JNK, p38 and ERK activation as wild-type Act1 (Fig. 2e and supplementary Fig. 3b). However, IL-17A-induced gene expression, including *Cxcl1*, *Csf2* and *Tnf*, was substantially reduced in Act1-deficient MEFs transduced with ΔSEFIR1 and SEFIR1+5mt compared to wild-type Act1, at both the mRNA and protein levels (Fig. 2f and Supplementary Fig. 3c). We examined whether ΔSEFIR1 and SEFIR1+5mt might be defective in mediating mRNA stabilization. The *Cxcl1*, *Csf2* and *Tnf* mRNAs were induced to similar levels in Act1-deficient MEFs reconstituted with wild-type Act1, ΔSEFIR1 or SEFIR1+5mt after the initial treatment with TNF (data not shown). However, the *Cxcl1*, *Csf2* and *Tnf* mRNAs decayed more rapidly in

Act1-deficient MEFs reconstituted with ΔSEFIR1 and SEFIR1+5mt than that with wild-type Act1 (Fig. 2g and Supplementary Fig. 3d). We then examined the possible binding of Act1 SEFIR to the 3' UTRs of *Csf2* and *Tnf*. Act1 SEFIR but not ΔSEFIR1 or SEFIR1+5mt bound the *Csf2* 3'UTR (nt 716–1010) and *Tnf* 3'UTR (nt 1362–1507) with similar affinity as the *Cxcl1* 3' UTR (Supplementary Fig. 3e). Furthermore, enriched *Cxcl1*, *Csf2* and *Tnf* mRNAs were detected in Act1 immunoprecipitates compared to that from IgG immunoprecipitation control in Act1-deficient MEFs restored with wild-type Act1, but not with ΔSEFIR1 or SEFIR1+5mt (Fig. 2h and Supplementary Fig 3f).

As controls, we also examined the impact of Act1-Rmt mutant (lost binding to IL-17RA) and Act1-Tmt (lost binding to TRAF6[27]) on mRNA stabilization. Act1-Rmt mutant completely lost IL-17A-induced signaling and impaired IL-17A-induced gene expression (Fig. 2d-f and Supplementary Fig. 3c), while Act1-Tmt (lost binding to TRAF6) failed to activate NFkB with partially reduced gene expression in response to IL-17A stimulation (Fig. 2d-f and Supplementary Fig. 3c). Notably, enriched *Cxcl1*, *Csf2* and *Tnf* mRNAs were readily detected in Act1 immunoprecipitates compared to that from IgG immunoprecipitation control in Act1-deficient MEFs restored with wild-type Act1 and Act1-Tmt, but not in Act1-Rmt MEFs in response to IL-17A after TNF pretreatment (Fig. 2h and Supplementary Fig. 3f). These results indicate that the recruitment of Act1 to IL-17RA is required for IL-17A-induced Act1-RNA binding in the cells, whereas Act1' binding to TRAF6 (and ability to activate NFkB) is independent from Act1's RNA binding activity. Consistently, IL-17A stimulation was able to stabilize *Cxcl1*, *Csf2* and *Tnf* mRNAs in Act1-deficient MEFs reconstituted with wild-type Act1 and Act1-Tmt, but not with Act1-Rmt (Fig. 2g and Supplementary Fig. 3d).

Act1 SEFIR binds to a stem-loop structure in *Cxcl1* 3'UTR

Consistent with the fact that Act1 SEFIR bound nt 720–940 (*Cxcl1* 220, Fig. 2b and 3a), wild-type Act1, but not Act1 mutants of ΔSEFIR1 and ΔSEFIR, stabilized reporter mRNA under the control of 3'UTR- *Cxcl1* 220 in the HeLa Tet-Off cells (Supplementary Fig. 4a). Act1 SEFIR bound nt 780–900 (*Cxcl1* 120) of *Cxcl1* 3' UTR with similar affinity (Fig. 3a-b). Secondary structure prediction (RNAfold web server, at http://rna.tbi.univie.ac.at/cgi-bin/RNAWebSuite/RNAfold.cgi) indicated that nt 780–900 might form a secondary structure with four stem-loops (named as A-D, Fig. 3b). We narrowed down the Act1-binding region to nt 810–857 (*Cxcl1* 47, Fig. 3a-b), which is an evolutionally conserved region retaining stem-loop B and C (Fig. 3a), designated as SEFIR binding element (SBE) (Fig. 3a and 3c). The binding of Act1 with SBE was confirmed by Surface Plasmon Resonance which revealed a Kd of 59.5nM (Supplementary Fig. 4b). While the disruption of stem-loop B had no impact on Act1 SEFIR's binding, impairment of stem-loop C completely prevented the binding of Act1 SEFIR (Fig. 3c). Likewise, IL-17A stimulation failed to attenuate *Cxcl1* mRNA decay in HeLa Tet-Off cells transfected with stem-loop C mutant (Fig. 3d). Taken together, the structure-function data implicate that Act1 SEFIR's binding to stem-loop C in the 3' UTR of *Cxcl1* is required for IL-17A-induced *Cxcl1* mRNA stabilization.

To further map the Act1-SEFIR binding site, we performed enzymatic RNA footprinting on the Act1 SEFIR-SBE complex. Nucleotides involved in the Act1-SBE interaction were

identified through partial digestion of the SBE RNA, which was performed in the absence or presence of Act1-SEFIR. The native RNA and RNA: protein complexes were then partially digested with different ribonucleases and analyzed by electrophoresis. The cleavage results with the native RNA (Fig. 3e, left panel) are consistent with the predicted structure shown in Figure 3c. RNase A cleaves at single-stranded C and U bases (yellow in Fig. 3f). RNase T1 cleaves after single-stranded G bases (purple in Fig. 3f). RNase V1 cleaves in double-stranded regions (blue in Fig. 3f). Several nucleotides (U19, C31, and U33) were cleaved with both single-stranded and double-stranded nucleases, suggesting that these regions may breathe. When the SBE was incubated with Act1-SEFIR, we observed partial protection of specific nucleotides from cleavage by RNase A (U36, U41–44); and RNase V1 (27–29, C31, 36–40) (Fig. 3e). Minor protection between nucleotides 19–23 was occasionally observed but this was not consistent between experiments. Interestingly, bases U10–12 became more accessible to RNase A cleavage which suggests that Act1 binding to stem loopC may cause conformational changes in stem loop B (bracket in Fig. 3e).

Taken together, the footprinting results validated that stem-loop C is the contact site for Act1 SEFIR. Disruption of the stem in stem-loop C (replacing CCC to GGG) abolished the binding of Act1 SEFIR to RNA, whereas replacement of the sequence in the stem of stem-loop C did not alter the binding of Act1 SEFIR, indicating that it is the secondary structure rather than the primary sequence that plays a critical role for Act1 SEFIR's recognition (Fig. 3g). However, the replacement of the entire loop TAA of the stem-loop C with AGU (without affecting the formation of the stem-loop) also abolished the SEFIR binding, demonstrating the importance of loop sequence for Act1 SEFIR-RNA binding (Fig. 3g).

Act1-RNA binding to 3'UTR inhibits decapping

The next question is how Act1-RNA binding in Dcp1-containing P-bodies mediates IL-17A-induced stabilization of otherwise unstable mRNAs of pro-inflammatory genes. mRNAs are decapped by the Dcp1/Dcp2 decapping enzymes and then degraded 5' to 3' by the exonuclease Xrn1[28, 29]. Since both co-immunoprecipitation and in situ PLA showed that Act1 binds to Dcp1, we examined whether Act1 binding to Dcp1 would affect decapping activity of Dcp1/Dcp2 complex. Purified Dcp1/Dcp2 and Act1 from transfected HeLa cells were incubated with the capped *Cxcl1* 3'UTR (nt 720–940). There was indeed dose-dependent inhibitory effect of Act1 (but not ΔSEFIR) on decapping efficiency of Dcp1/Dcp2 complex (Fig. 4a, 4b and Supplementary Fig. 5a). Additionally, Act1 failed to protect the stem-loop C transcript from decapping, confirming the importance of Act1-RNA binding for the Act1's inhibition of decapping (Fig. 4a and 4b).

Act1 brings TBK1 to disrupt the decapping complex via phosphorylation of Dcp1

IL-17A stimulation induced Dcp1 phosphorylation at S315 (Fig. 4c), which was shown to be required for the inactivation of the decapping activity[30, 31]. While recent studies reported two Act1-interacting kinases: IKKi and TBK1[32, 33] (Fig. 4d), IL-17A induced the interaction of only TBK1 (but IKKi) with Dcp1 (Fig. 4c, Supplementary Fig. 1d-f and data not shown). IL-17A-induced Dcp1 phosphorylation (but no p-p65) was diminished in TBK1-deficient cells, whereas IKKi deficiency had little effect (Supplementary Fig. 5b). Recombinant TBK1 was able to phosphorylate Dcp1 in an *in vitro* kinase assay (Fig. 4e). TBK1 inhibitor

blocked IL-17A-induced phosphorylation of TBK1/Dcp1 without affecting the interaction of TBK1 with Act1 or Dcp1, suggesting that TBK1 activation is not required for its interaction with Act1-Dcp1 complex (Fig. 4c). TBK1 overexpression diminished the interaction between Dcp1 and Dcp2, while TBK1 failed to remove Dcp1 S315A mutant from Dcp2 (Supplementary Fig. 5c). Furthermore, TBK1 inhibitor effectively abolished Act1-mediated inhibition of decapping (Fig. 4a and 4b) and TBK1, but not IKKi immunodepletion abolished Act1-mediated inhibition of decapping (Supplementary Fig. 5d-e). Consistently, TBK1 deficiency substantially reduced IL-17A-induced expression of *Cxcl1*, *Csf2* and *Tnf* at both mRNA and protein levels (Fig. 4f). Taken together, these results suggest that Act1 may bring TBK1 to the mRNA targets in the P-bodies where TBK1 phosphorylates Dcp1, resulting in Dcp1 dissociation from Act1-RNP, inhibition of decapping and stabilization of mRNAs.

Act1 forms distinct RNPs with Dcp1, Dcp2, SF2 and HuR

Our results described here have defined an Act1-RNP consisting of Act1-TBK1-Dcp1/2, which was designated as RNP2. While imaging studies indicated that SF2 and HuR were not co-localized with Dcp1 (Supplementary Fig. 1c), we performed immunoprecipitation experiments to examine the different Act1-RNPs. While IL-17A induced Dcp1-Act1-TBK1 interaction in an RNA-dependent manner (sensitive to RNase treatment), SF2 and HuR were not detected in this RNP (RNP2) (Supplementary Fig. 1d). IL-17A-induced Act1-SF2 complex (RNP1) was also sensitive to RNase pretreatment, but Dcp1-TBK1 and HuR were not found in this Act1-SF2-RNP (Supplementary Fig. 1e). Likewise, we failed to detect Dcp1-TBK1 and SF2 in IL-17A-induced Act1-HuR RNP (RNP3, Supplementary Fig. 1f). Taken together, these results suggest that the Act1-SF2, Act1-Dcp1/2 and Act1-HuR represent three independent RNPs. Deletion of SEFIR1 (ΔSEFIR1) abolished the formation of all three RNPs, implicating the importance of Act1's binding to mRNA for the formation of these Act1-RNPs (Supplementary Fig. 1d-f).

SF2 has been shown to mediate decay of cytokine and chemokine mRNA[34, 35]. We reported that SF2 bound chemokine mRNA (induced by TNF) in the absence of IL-17A stimulation[36], whereas the SF2-mRNA interaction was much reduced after stimulation with IL-17A in an Act1-dependent manner (Fig. 5a and Supplementary Fig. 6a). Interestingly, we now found that IL-17A failed to reduce SF2's binding to *Cxcl1* in Act1-deficient cells restored with ΔSEFIR1, suggesting that Act1's RNA binding might be required for the dissociation of SF2 from the mRNAs (Fig. 5a). One important question is how Act1's binding to mRNAs promotes the dissociation of SF2 from the mRNAs. We found that SF2 was able to bind the same region on *Cxcl1* as Act1: the SEFIR binding element (SBE); and the impairment of stem-loop C completely prevented the binding of SF2 (Fig. 5b and Supplementary Fig. 6b). Addition of increasing amounts of Act1 to the RNA binding reaction attenuated SF2's binding to SBE (Fig. 5c). Notably, SF2 phosphorylation has been implicated as a mechanism for its dissociation from mRNA targets[37]. While both imaging and fractionation experiments indicated that Act1-SF2 RNP1 resides in the nucleus (Supplementary Fig. 1c and 6c), IKKi (a kinase required for IL-17A-mediated mRNA stabilization[32] was translocated into the nucleus and detected in the Act1-SF2 RNP1 in response to IL-17A stimulation (Supplementary Fig. 6c). IKKi indeed was able to

phosphorylate SF2 in vitro (Fig. 5d) and incubation of recombinant IKKi with SF2 reduced the ability of SF2 to bind *Cxcl1* mRNA (Supplementary Fig. 6d), implicating IKKi in preventing SF2's binding to mRNAs. Whereas IL-17A-induced IKKi-SF2 and Act1-SF2 interaction were abolished in Act1-deficient MEFs restored with ΔSEFIR1 (Fig. 5a and Supplementary Fig. 6c), Act1-IKKi interaction in both cytosol and nucleus was retained in these cells (Supplementary Fig. 6c). These results suggest that IL-17A induces Act1-IKKi interaction prior to their translocation to the nucleus and Act1's binding to SF2-bound mRNAs in the nucleus allows IKKi to phosphorylate SF2, attenuating SF2's binding to the mRNA targets.

HuR was implicated in shifting target mRNAs to polysomes for protein translation and IL-17A stimulation induced the co-shift of Act1-HuR to the polysomes[20, 38]. IL-17A induced the binding of HuR to *Cxcl1* in Act1-expressing MEFs, which was abolished in Act1-deficient MEFs restored with ΔSEFIR1, suggesting that Act1's RNA binding might also be required for HuR's recruitment to the target mRNAs (Fig. 5a). We found that HuR bound to CXC1 220-I, but not CXC1 220-II (Fig. 5b and Supplementary Fig. 6e). HuR and Act1 can simultaneously bind to CXC1 220 (Fig. 5e). Removal of nt 720–829 from CXC1 220 abolished HuR binding, whereas Act1 binding was retained, indicating that HuR and Act1 have their independent binding sequences on *Cxcl1* (Fig. 5b and 5e). Since HuR is not part of RNP1 (Act1-SF2) (Supplementary Fig. 1c-f), Act1 may facilitate HuR's binding to *Cxcl1* in vivo after competing off SF2 from target mRNAs. In support of this, IL-17A-induced the co-shift of Act1-HuR to the polysomes[20] was abolished in Act1-deficient MEFs restored with ΔSEFIR1 (Fig. 5f-g). The ratio of *Cxcl1* mRNA in the translation active polysomes over the inactive fractions was substantially reduced in Act1-deficient MEFs restored with ΔSEFIR1 (Fig. 5g-h). Based on these results, we propose the following model for the actions of Act1-RNA binding (Supplementary Fig. 1h): First, IL-17 induces Act1's binding to the mRNAs (such as *Cxcl1*) in the nucleus (RNP1) preventing SF2-mdiated mRNA decay by competing off SF2's binding to the mRNAs which is further promoted by IKKi-mediated SF2 phosphorylation. Second, Act1 follows the mRNAs to the P-bodies (RNP2) inhibiting Dcp1/2-mediated mRNA decapping by employing TBK1 to phosphorylate Dcp1. Lastly, Act1-mRNAs are shifted to the polysomes by facilitating HuR's binding to mRNAs (RNP3) for protein translation.

SBE RNA aptamers abolished IL-17A-induced mRNA stabilization of *Cxcl1*, *Csf2* and *Tnf*

We then hypothesized that RNA oligonucleotides corresponding to the SBE (SEFIR Binding Element) might inhibit the effect of Act1 in the defined RNPs and inflammatory gene expression. SBE RNA aptamer and mutant stem-loop B aptamer (but not mutant stem-loop C) were able to compete off Act1 SEFIR's binding to the *Cxcl1* 3'UTR (Fig. 6a). The transfected fluorescent SBE RNA aptamers mainly resided in the cytoplasm and was detected in Act1 granules (Fig. 7b and Supplementary Fig. 6a). Act1 granules were substantially reduced over time in cells transfected with SBE RNA aptamers, implicating that this SBE RNA aptamers might be disrupting the Act1's co-localization with the P-bodies (Fig. 6c). SBE RNA aptamers, but not SBE aptamers with mutated stem-loop C, abolished the formation of Act1 granules and Act1's co-localization with Dcp1 (Fig. 6c). Furthermore, SBE RNA aptamers specifically disrupted endogenous Act1-Dcp1 and Act1-

HuR interaction in the cytoplasm but had no effect on Act1-SF2 interaction in the nucleus (Supplementary Fig. 7b), which is consistent with the fact that SBE RNA aptamers mainly resided in the cytoplasm (Fig. 6b and Supplementary Fig. 7a). SBE RNA aptamers was also able to compete off Act1 SEFIR's binding to the 3' UTRs of *Csf2* and *Tnf* (Fig. 6d and Supplementary Fig. 7c), suggesting that the binding of SBE RNA aptamers to Act1 SEFIR blocks Act1's binding to the mRNA targets. These results suggest that the SBE RNA aptamers has the potential to be an inhibitory agent for blocking IL-17A-induced inflammatory response. We indeed found that transfection of SBE RNA aptamers reduced IL-17A-, IL-17E-, but not IL-1-mediated mRNA stabilization and the production of CXCL1, GM-CSF and TNF (Fig. 6e-f and Supplementary Fig. 7d-g).

SBE RNA aptamers inhibited IL-17A-dependent skin and lung inflammation

Secukinumab (anti-IL-17A) showed great efficacy for psoriasis and has been approved by FDA for treatment of psoriasis. Aberrant keratinocyte proliferation and neutrophilic inflammation are well-known hallmarks of pathogenesis of psoriasis. We found that SBE RNA aptamer, but not mutant aptamer substantially reduced IL-17A-dependent epidermal hyperplasia and neutrophil infiltration in the ears (Fig. 7a-c). Likewise, SBE RNA aptamer, but not mutant aptamer greatly diminished IL-17A-induced expression of *Cxcl1, Csf2 and Tnf* in the ears (Fig. 7d). Taken together, these data indicate that IL-17A induces keratinocytes proliferation and neutrophil infiltration, resulting in epidermal hyperplasia, which were effectively blocked by SBE RNA aptamers.

House dust mite (HDM), a natural allergen to which asthmatics are often sensitized, can induce neutrophilic airway inflammation, which is often associated with severe asthma[39]. Consistent with the literature, we found that IL-17RC$^{-/-}$ (but not IL-17RB$^{-/-}$) mice substantially reduced neutrophilic airway inflammation in a high-dose HDM-induced severe asthma model ([40] and data not shown), during which IL-17 (bot not IL-17E) was highly induced (Fig. 7f). Tracheal section of mice subjected to intranasal administration of fluorescently-labeled SBE RNA aptamers showed efficient tissue penetration of SBE RNA aptamers (Fig. 7e) and their co-localization with Act1 inside the cells (Fig. 7e). We then evaluated the ability of SBE RNA aptamers in alleviating neutrophilia in this IL-17A-dependent severe asthma model. HDM-induced neutrophilia and inflammatory gene expression in the BAL and lung were substantially reduced by treatment SBE RNA aptamers (Fig. 7g-j). Taken together, results from HDM experiments indicate the potential therapeutic role of SBE RNA aptamers in treatment of IL-17A-mediated severe asthma.

Discussion

The SEFIR domain, a conserved motif present in the cytoplasmic regions of IL-17 receptor subunits and adaptor Act1, mediates the recruitment of Act1 to the receptor upon IL-17 stimulation. Here we have unexpectedly identified SEFIR of Act1 as a direct RNA binding domain, rendering Act1 RNA binding activity to stabilize otherwise unstable mRNAs of the pro-inflammatory genes (*Cxcl1*, *Csf2* and *Tnf*) in response to IL-17 stimulation. Act1 directly binds to the 3'-UTRs of inflammatory mRNAs to form distinct RNPs in several subcellular compartments including P-bodies controlling mRNA metabolism. Structure-

function analysis showed that Act1 SEFIR binds to a stem-loop structure (named as SBE) in the *Cxcl1* 3'UTR. RNA aptamers containing SBE abolished Act1's binding to the target mRNAs and attenuated IL-17-mediated mRNA stabilization. Furthermore, SBE RNA aptamers inhibited IL-17A-induced skin inflammation and reduced airway inflammation in house dust mite-induced asthma model. Taken together, this study demonstrates that the receptor-proximal adaptor Act1 directly binds to mRNAs to control the steps of RNA metabolism, which provides a novel molecular mechanism of inflammatory response via receptor-specific mRNA stabilization of select inflammatory genes. Moreover, the discovery of a non-canonical function of Act1 will allow the development of new therapeutic strategies for autoimmune inflammatory diseases.

We and others have previously shown that Act1 is required for IL-17R-mediated signaling including NFkB, JNK, p38 and ERK[13]. The Act1 mutants defective in RNA binding retained the ability to interact with IL-17RA and were able to mediate IL-17-induced NFkB, JNK, ERK and p38 activation. These data indicate a novel function of Act1 as a RNA binding protein for mRNA stabilization, which can be segregated from its role as an adaptor. Using Act1 mutants defective in binding to the receptor or TRAF6, we found that the recruitment of Act1 to IL-17RA is required for IL-17-induced Act1-RNA binding in the cells, whereas Act1' binding to TRAF6 (and ability to activate NFkB) is independent from Act1's RNA binding activity. It is intriguing that this study reveals the selective recruitment of IKKi to Act1 RNP1 (SF2 complex) and TBK1 to Act1 RNP2 (Dcp1 complex). Additionally, TBK1, but not IKKi was required for IL-17-induced Dcp1 phosphorylation. Recent studies imply that distinct scaffold proteins assemble TBK1 and IKKi subcomplexes, in a stimulus-specific manner, which might be a mechanism to achieve specificity[41, 42, 43, 44].

Taken together, we propose the following model for the actions of Act1-RNA binding for IL-17-induced inflammatory response. Upon IL-17 stimulation, multiple signaling pathways (including NFkB and MAPKs) are activated to induce the gene transcription of cytokines and chemokines. Act1 then directly binds the mRNAs of cytokines and chemokines to stabilize these otherwise unstable mRNAs for the production of the pro-inflammatory mediators. Act1's binding to mRNAs of inflammatory genes results in the formation of multiple RNPs controlling different steps of mRNA metabolism. The study here provides the first example of a receptor-interacting adaptor molecule, Act1, playing a direct role in mRNA metabolism, orchestrating receptor-mediated selectivity of mRNA stabilization and translation. Considering the efficacy of SBE RNA aptamers in blocking IL-17-dependent skin and airway inflammation, this newly found mechanism of Act1 also provides an opportunity to develop IL-17-Act1 targeted new therapeutic agents for treating inflammatory diseases.

Materials and methods

Animals:

IKKi-deficient mice were a gift from T. Maniatis. TBK1 flox mice were obtained from Millenium Pharmaceuticals, Inc., Mice 6 weeks of age were used for primary kidney cells isolation. LSL–HA–Act1 knock-in mice were bred onto UBC-Cre-ERT2 mice[45]. All mice

were on the C57BL/6 N background; all protocols were approved by the Cleveland Clinic Institutional Animal Care and use Committee; and all studies were executed by following relevant ethical regulations detailed in animal use protocols.

Cell culture and Reagents:

The following antibodies were used: Santa Cruz Biotechnology: anti-Act1 (sc-11444, clone H300), anti-HuR (sc-5261, clone 3A2), anti-SF2 (anti-28724, clone H-110), GAPDH (sc-47724, mouse monoclonal), anti-β-actin (sc-8432, mouse monoclonal). Sigma anti-HA (H-9658, mouse monoclonal). Cell Signaling Technology: anti-TBK1 (3504, clone D1B4), anti-M2 (2368, rabbit polyclonal), anti-V5 (13202, rabbit polyclonal), anti-p-JNK (9251, rabbit polyclonal), anti-JNK (9252, rabbit polyclonal), anti-p-IkB (2859, clone 14D4), anti-p-p65 (3033, clone 93H1), anti-p65 (8242, clone D14E12), anti-Ikki (3416, clone D61F9), anti-p-IKKα/β (2697, clone 16A6), anti-pERK (3371, rabbit polyclonal). p-S315 Dcp1a antibody was kind gift from Dr. Elisa Izaurralde. Dcp1 antibody was kind gift from Dr. Jens-Lykke Andersen. TBK1 inhibitor MRT67307 was purchased from Sigma Aldrich. Primary MEFs were isolated from wild-type, Act1-deficient and LSL–HA–Act1 knock-in /UBC-Cre-ERT2 embryos at embryonic day 14. Cell culture of mouse embryonic fibroblasts (MEFs), HeLa Tet-Off cells and primary kidney epithelial cells was performed as previously described[20, 24]. Proximity-based ligation assays were performed in Hela cells according to the manufacturer's instructions (Duolink™Assay, Sigma Aldrich).

When stimulated ex vivo, cells were stimulated with mouse IL-17A (50 ng/ml, 421-MT, R&D Systems), human IL-17A (50 ng/ml, 317–1ML, R&D Systems), mouse TNFα (10ng/ml, 410-MT, R&D Systems), IL-1 (10 ng/ml, 201-LB, R&D Systems) or IL-25E (10 μg/ml, 1399-IL, R&D Systems).

Transfection, adenoviral and retroviral infection:

Transfections of HeLa cells were conducted with Lipofectamine 2000 (Invitrogen) according to the manufacturer's instructions. For Act1 reconstitution into Act1−/− MEFs and transfection of LSL–HA–Act1 knock-in /UBC-Cre-ERT2 MEFs, cells were either infected by retroviral supernatant as described previously[12] or transfected using Amaxa nucleofector apparatus (Amaxa, GmbH, Cologne, Germany). Supernatants for retroviral infections were obtained by transfecting Phoenix cells with 5 μg of retroviral constructs derived from pMSCV-IRES-GFP for 48 hours. MEFs were infected with viral supernatant for 24 hours and GFP-positive cells were sorted out to establish stable cell lines for downstream assay. Transfections using Amaxa nucleofector apparatus were performed according to the manufacturer's instructions (program A-023, Amaxa MEF nucleofector Kit 1).

Quantitative real-time PCR:

Total RNA was isolated with TRIzol reagent (Invitrogen). The cDNA was synthesized with random hexamers (Applied Biosystems) and M-MLV reverse transcriptase (Promega). Real-time PCR was performed using a SYBR Green PCR Master Mix kit (Applied Biosystems). All gene expression results were calculated by the change- in-cycling-threshold (ΔCT) method, where ΔCT = CT of target gene − CT of *Actb* (encoding β-actin), and are presented as 2–ΔCT. The primers used for qPCR are listed in Supplementary Table 1.

Constructs:

For GFP reporter constructs, full-length cDNAs of hAct1, hDcp1a, hIKKi, hTBK1 and hTIA1 were cloned into pEGFP-N1 vector (Clontech). For RFP reporter constructs, full-length cDNAs of hAct1, hIRAK1, and hDcp1a were cloned into pDsRed-Monomer-Hyg-N1 vector (Clontech). For constructs V5-hDcp1a, FLAG-hDcp1a, FLAG-hDcp2, FLAG-hIRAK1, V5-IL-17RA, HA-hAct1 and HA-hAct1ΔSEFIR, the cDNAs with the corresponding tag were cloned into pcDNA3.1 vector. Wild-type (FLAG-hAct1) and Act1 internal deletion mutants of the SEFIR domain [designated ΔSEFIR1 to ΔSEFIR5 (based on the five exons that encode regions of the SEFIR domain: 410 to 439, 440 to 462, 463 to 501, 502 to 526, and 527 to 552) and ΔSEFIR (deletion of amino acid residues 391 to 537)], receptor binding mutant[41] (H472D), TRAF6 binding mutant[41] (deletion of amino acid residues 38–42, 333–337) or RNA binding mutant (SEFIR1+5mt) (K407A, K524A, K526A, and K527A) were flag-tagged and cloned into pcDNA3.1. Retroviral Act1-WT and Act1 mutant constructs derived from pMSCV-IRES-GFP were described before[6, 12, 24].

Constructs for in vitro transcription:

Fragments containing the 3'UTR sequences of CXCL1 220 (nt 720–940) and the truncated fragments CXCL1 120 (nt 780–900), CXCL1 110 (nt 780–890), CXCL1 90 (nt 790–880), CXCL1 80 (nt 800–880), CXCL1 70 (nt 800–870); SBE WT (CXCL1 47, nt 810–857), SBE mutant B (CXCL1 47, nt 810–857 with altered sequence shown in Table 2), SBE mutant C (CXCL1 47, nt 810–857 with altered sequence shown in Table 2), Stem-loop B (CXCL1, 800–835) and Stem-loop C (CXCL1, 830–856) and as well as 3'UTR sequences of TNF (nt 1361–1507), GM-CSF (nt 513–785) and GPx1 (nt 775–962) were generated by PCR and cloned into pGEM-3ZF(+) vector (Promega) using EcoRI and BamHI sites. The plasmid containing 3'UTR of mouse TNF were kind gift of Dr. Vigo Heissmeyer. All mutations were introduced using QuikChange II Site Directed Mutagenesis Kit (Stratagene) according to the manufacturer's instructions. Primers used for generating all constructs are listed in Supplementary Table 2.

In vitro transcription and cap-labeling:

REMSA radiolabeled 3' UTR RNA probes were synthesized from BamHI linearized plasmids (see constructs for *in vitro* transcription) templates with T7 RNA polymerase using 1 mM GTP, 1 mM ATP, 1 mM CTP, 0.005 mM UTP and 25 μCi of 32P-labeled UTP for 3 hours at 37°C. Probes were DNAse I treated for 20 minutes and then phenol:chloroform extracted. The aqueous phase was passed through a Micro Bio-Spin P30 column according to manufacturer's instructions (BioRad). For *in vitro* decapping probes were synthetized as above, but using un-labeled 1 mM CTP, DNAse treated and purified. Cap-labeling was performed using the vaccinia capping system (NEB) according to the manufacturer's instructions in the presence of [α−32P] GTP.

For RNase footprinting experiments, cold synthetic transcripts were dephosphorylated with SuperSAP (Affymetrix), purified, and resuspended in nuclease-free water. Dephosphorylated transcripts were end-labeled in the presence of [γ^{32}P] ATP (3000 Ci/mmole; Perkin Elmer Easy Tides) and T4 PNK (NEB) at 20 units/pmole RNA. The transcripts were gel purified on 8% acrylamide (19:1)/7M urea gels and eluted in 10 mM Tris HCl, pH 7.5, 1 mM EDTA,

pH 8, 300 mM NaAc, pH 5.5 at 4°C overnight. Purified RNA was stored in 10 mM Tris HCl, pH 7.5 at −20°C.

RNase footprinting

End-labeled ^{32}P-labeled CXCL1 SBE RNA was heated to 95°C and slow cooled to room temperature. The RNA (2.5 nM) was incubated in L30 binding buffer (30 mM Tris HCl, pH 8.0, 75 mM KCl, 5 mM $MgCl_2$, 1 mM DTT, 0.04 μg/μL BSA (NEB), 10% glycerol, and 50 ng/μL yeast tRNA) with or without mouse Act1 SEFIR protein (1.5 μM) at 30°C for 10 min. Reactions were cooled to room temperature over a 2 min period and then placed at 22°C for 2–5 min. The indicated amounts of RNase T1, A, or V1 (Ambion) were added to the appropriate samples and incubated at 22°C for 5 min. Enzymatic reactions were quenched with 30 μL Inactivation/Precipitation buffer (Ambion) and purified according to manufacturer's directions. Samples were resuspended in 10 μL of loading buffer (Ambion), heat-denatured at 95°C for 5 min, and separated in a denaturing 8% (19:1) polyacrylamide/7 M urea gel. The dried gels were visualized with a phosphorimager or on film.

Sequencing ladders were prepared by incubating end-labeled ^{32}P-labeled CXCL1 SBE RNA (2.5 nM) in 1X Sequencing Buffer (Ambion) supplemented with 50 ng/μL yeast tRNA. The RNAs were incubated at 50°C for 5 min, cooled to 22°C and the indicated amounts of RNase T1 and A added. The samples were incubated, quenched, and purified as described above. Alkali ladders were prepared by incubating end-labeled ^{32}P-labeled PHGPx SECIS RNA (2.5 nM) in 100 mM NaOH, 2 mM EDTA, pH 8.0, and 2 μg/μL yeast tRNA at 37°C for 3 min, to which 0.2 M Tris HCl, pH 8.0 (final) was added. The samples were frozen on dry ice and combined with an equal volume of loading buffer.

RNA Electrophoretic Mobility Shift Assay (REMSA):

Increasing amounts of purified protein and labeled probes (10 fmol, see in vitro transcription) were combined in the binding buffer for 30 minutes. The final REMSA binding buffer concentrations were 140 mM KCl, 10 mM HEPES pH 7.9, 5% glycerol, 1 mM DTT and 0.33 mg/ml tRNA. The reaction was further supplemented with 15 μg salmon sperm DNA to reduce non-specific interactions from the lysate. Complexes were resolved on either 4% or 6% non-denaturing polyacrylamide gels. The gels were dried and the appearance of complexes was visualized by exposure to BioMax MR film. Dissociation constants (*Kd*) were determined by quantified the protein- bound fractions using ImageJ software and plotted against protein concentration (nM). *Kd* values were extracted from plots fitted to a hyperbolic function in Graph PAD Prism software (OriginLab).

SBE aptamers Competition:

The purified recombinant His-MBP-Act1 SEFIR (200ng) was incubated with the ^{32}P-labeled *Csf2* and *Tnf* 3'UTR probes for 15mins to form Protein: RNA complex. Cold RNAs were added at 0, 25, 50, 100 or 200-fold molar excess over the probe for additional 10 mins, followed by REMSA. SBE WT (*Cxcl1* 47 as indicated in Fig. 3a) and SBE mutant C were used in the competition assay (Fig. 7a and d). IC50 is calculated as the concentration of aptamers that displace 50% of bound *Cxcl1* 220 probe from the Act1-SEFIR.

Protein Modeling:

The structure model of Act1-SEFIR was built by SWISS-Model (http://swissmodel.expasy.org), using the crystal structure of IL- 17RA-SEFIR as the template [46] (PDBcode:4NUX).

Surface Plasmon Resonance:

Binding affinity of SPR was conducted on a Biacore 3000. The biotinylated RNA was immobilized on a streptavidin-coated sensor chip. SA sensor chips was activated and blocked according to standard protocols. RNA was diluted to 1 mM in HBS-EP buffer (10 mM HEPES, pH 7.4, 150 mM NaCl, 3mM EDTA, 0.005% surfactant P20) heated at 80 °C for 10 min, cooled to room temperature to allow annealing of the stem, diluted 500-fold in running buffer. RNA was injected at a flow rate of 10 μL/min ~ 40 resonance units of RNA were captured on the SA chip. To study the RNA /Act1 interactions, the proteins were diluted in running buffer and injected at the concentrations indicated in the sensorgrams. Binding experiments were carried out at 25 °C and a flow rate of 30 μl/ min. Any protein that remained bound after a 3-min dissociation phase was removed by injecting 2 M NaCl for 60 s at 20 μl/ min, which regenerated the RNA surface completely. Data were analyzed with BIAcore 3000 evaluation software and curves were fitted with the “1:1 binding with drifting baseline” model.

Immunodepletion of endogenous TBK1 and IKKi:

TBK1- or IKKi-depleted extracts were prepared by incubating extracts of 2×10^6 of HeLa cells with 25 μl protein G beads (pre-incubated with 5 ug of either anti-TBK1 or anti-IKKi antibodies) at 4°C for 4 hours. The beads were then separated from the extract by centrifugation 3,000 × g for 2 min at 4°C and supernatants were used for protein purification.

Decapping assays:

Dcp1/Dcp2 complex and Act1 protein were purified from HeLa cells (2×10^6) either co-transfected with 10 μg of FLAG-tagged Dcp1 and FLAG-tagged Dcp2 (kind gift from Dr. Andersen) or with 10 μg of FLAG-tagged Act1 by using anti-FLAG/M2-beads (Sigma), eluted in 50 μl using 3 × FLAG peptide (Sigma) and protein concentrations were estimated by comparison to a Act1 SEFIR protein of known concentration. 10 fmol of [^{32}P] cap-labeled RNA substrate was incubated with the purified Dcp1/Dcp2 complex (100 ng of each protein) and increasing amounts of purified Act1 protein (0, 100 and 300 ng) in decapping buffer (10 mM Tris, pH 7.5, 100 mM KOAc, 2 mM MgOAc, 2 mM DTT) supplemented with fresh 0.5 mM MnCl2 for 30 min at 370C. The reaction was terminated by addition of 1 μl of 0.5M EDTA. Reaction products were separated and identified by TLC on cellulose sheets developed in 450 mM (NH4)2SO4. 7meGMP and 7meGDP (20 μg) were spotted routinely on TLC plates along with reaction samples to serve as markers that could be visualized by UV shadowing.

Intradermal injection:

LSL–HA–Act1 knock-in /UBC-Cre-ERT2 mice were injected with tamoxifen (~5 mg/25 g weight) 14 and 7 days prior to Intradermal experiment. The ears of 8-week-old female mice were injected intradermally with 20 μl of PBS alone or with PBS containing 0.5 mg of recombinant mouse IL-17A in the presence or absence of 5 nmol of either SBE WT aptamer or SBE mutant C aptamer (for sequence see Table 2). Mice were injected daily for 6 consecutive days. Six days after injection, skin tissue was collected for RNA and staining analyses. For H&E and DAB (3,3′-diaminobenzidine, BD phamagen) staining, skin tissue was fixed in 10% formalin and then processed into paraffin blocks. Epidermal thickness was quantified by ImageJ software.

HDM-induced asthma:

Eight-week-old female WT C57BL/6 mice were sensitized sub-cutaneously with HDM (100 mg per mouse; Dermatophagoides farina, Greer Laboratories) in complete Freund's adjuvant (CFA) on day 0 and subsequently challenged (intranasally) with HDM (100 mg per mouse) on day 14. One hour before last HDM challenge mice were administered intranasally with either SBE WT or SBE mutant C aptamer mixed with 5 μl of TransIT-TKO reagent (Mirus Bio) and PBS in a total volume of 40 μl. We equally divided aptamer mix and into two nostrils and applied with a micropipette. Each mouse received 5 nmol of aptamer. BAL cell counting, and tissue collection were performed 24 hours after the last HDM challenge.

For monitoring aptamer delivery into trachea fluorescently-labeled SBE WT aptamers were intranasally delivered to tamoxifen treated LSL-Act1-HA knock-in Cre-ERT2 mice (see **Intradermal injection**).

Aptamer design:

Aptamers containing sequences of SBE WT and SBE mutant C (see Supplementary Table 3) were ordered form Integrated DNA Technologies. Three first residues form both 5' and 3'end were methylated (2′-O- Methyl RNA bases) in order to enhance stability. For detection, aptamers were further modified at 5' end with either 6-FAM or Atto647 fluorescent dyes.

Histological analysis:

Tracheas were collected from LSL-Act1-HA KI Cre-ERT2 mice subjected to intranasal administration of fluorescently-labeled SBE RNA aptamers, snap-frozen in OCT medium and cryosectioned at 5 μm. Frozen tissue sections was fixed and permeabilized with 4% paraformaldehyde solution containing 0.2% Triton X-100 for 10 minutes. Sections were incubated with rabbit anti-HA Ab followed by staining with Alexa Fluor 488-conjugated goat anti-mouse Ab (green) and microscopic analysis.

ELISA assay:

Supernatants from cell cultures were collected and measured for the level of mouse cytokines CXCL1 and TNFα using Duoset ELISA kits (R&D system) according to manufacturer's instructions.

RNA-binding assays RIP:

The ability of Act1 to bind to RNA *in vivo* was assessed as described previously[47]. Briefly, 10×10^6 $Act1^{-/-}$ MEFs reconstituted by retroviral infection with M2-tagged mouse wild-type Act1 (WT) were left untreated or treated with IL-17 (50 ng/ml) for 1 hour. Cells were trypsinized, washed twice, and resuspended in 10 ml ice-cold PBS. Cells were fixed in 0.1% formaldehyde for 15 min at room temperature, whereupon the cross-linking reaction was stopped with glycine (pH 7; 0.25 M). The cells were then washed twice with ice-cold PBS, resuspended in 2 ml RIPA buffer (50 mM Tris-HCl [pH 7.5], 1% Nonidet P-40, 0.5% sodium deoxycholate, 0.05% SDS, 1 mM EDTA, 150 mM NaCl, and pro-teinase inhibitors), and sonicated. The lysate was centrifuged (15 min, 4 °C, 16,000 × g), and 1 ml each supernatant was immunoprecipitated overnight at 4 °C, using Dynabeads (invitrogen) preincubated with 20 μg anti-M2 or anti-IgG Ab. The beads were washed five times with 1 ml RIPA buffer and resuspended in 150 μl elution buffer (50 mM Tris-Cl [pH 7], 5 mM EDTA, 10 mM DTT, 1% SDS). Cross-linking was reversed by incubation at 70°C for 45 min, RNA was purified from immunoprecipitates with Trizol (Invitrogen) according to the manufacturer's instructions and treated with RNase-free DNase, the cDNAs were synthesized and 10% (two microliters) of the reverse transcriptase product was subjected to quantitative real-time PCR. Primers used for quantitative real-time PCR are listed in Supplementary Table 1.

RIP data analysis:

Ct value of each RIP RNA fractions was normalized to the Input RNA fraction Ct value for the same qPCR Assay (ΔCt) to account for RNA sample preparation differences. Then the normalized RIP fraction Ct value (ΔCt) was adjusted for the normalized background (anti-IgG) [non-specific (NS) Ab] fraction Ct value (ΔΔCt). The fold enrichment [RIP/non-specific (NS)] was calculated by linear conversion of the ΔΔCt. Below are the formulas used for the calculation: ΔCt [normalized RIP] = Ct [RIP] – (Ct [Input] – Log2 (fraction of the input RNA saved))); ΔΔCt [RIP/NS] = ΔCt [normalized RIP] – ΔCt [normalized NS]; Fold Enrichment = 2 (-ΔΔCt [RIP/NS]).

Immunoblot, immunoprecipitation and nuclear fractionation:

Cell were harvested and lysed on ice in a lysis buffer containing 0.5% Triton X-100, 20 mM Hepes pH 7.4,150 mM NaCl, 12.5 mM -glycerophosphate, 1.5 mM MgCl2, 10 mM NaF, 2 mM dithiothreitol, 1 mM sodium orthovanadate, 2 mM EGTA, 20 mM aprotinin, and 1 mM phenylmethylsulfonyl fluoride for 20 minutes, followed by centrifuging at 12,000 rpm for 15 minutes to extract clear lysates. For immunoprecipitation, cell lysates were incubated with 1 μg of antibody and A-sepharose beads at 4 degree overnight. After incubation, the beads were washed four times with lysis buffer and the precipitates were eluted with 2x sample buffer. Elutes and whole cell extracts were resolved on SDS-PAGE followed by immunobloting with antibodies. Nuclear fractionation was performed using NUCLEI EZ PREP kit purchased from Sigma in accordance with the manufacturer's instruction. Nuclear pellets were suspended in 30μl of nuclear extraction buffer (20 mM HEPES, 400 mM NaCl, 1 mM EDTA, 1 mM EGTA in water, pH 7.9) containing freshly prepared 1 mM DTT and protease inhibitor cocktail. After 1.5 h incubation on ice bath with intermittent vortexing,

extracts were centrifuged and supernatant was collected for immunoprecipitation. Uncropped gels can pertaining to all the Figs. can be found in Supplementary Fig. 8.

Expression and purification of His-IL-17RA SEFIR, His-MBP-mAct1-SEFIR and His-MBP proteins

The cDNA encoding a SEFIR domain–containing fragment of human IL17RA (His-IL-17RA SEFIR, aa residues 351 to 616) was subcloned into a modified pET-28 vector, with a N-terminal 6x His tag and a tobacco etch virus protease (TEV) recognition site (ENLYFQG). The IL17RA SEFIR domain was expressed and purified by double-Nickel-Nitrilotriacetic Acid (Ni-NTA) affinity methods as previously described[48]. Size exclusion chromatography on a superdex s200 high resolution column was used as a final step for purification. The cDNA encoding a SEFIR domain containing a fragment of mouse Act1 (aa residues 391 to 537) and its deletion mutants of the SEFIR domain, designated SEFIR1 to SEFIR5 (based on the five exons that encode regions of the SEFIR domain: 410 to 439, 440 to 462, 463 to 501, 502 to 526, and 527 to 552) was cloned into a modified pET28b vector that expresses maltose-binding protein (MBP) with an N-terminal 6x His tag and a C-terminal TEV recognition site. Recombinant mAct1-SEFIR or MBP protein was expressed and purified as previously described[49]. Size exclusion chromatography on a superdex s200 high resolution column was used as a final step for purification.

In vitro kinase assay:

Recombinant IKKi and TBK1 (100 nM) was incubated respectively with purified SF2 and Dcp1(10 nM) in the kinase assay buffer containing 25 mM Tris (pH 7.5), 5 mM β-glycerophosphate, 2 mM DTT, 0.1 mM Na_3VO_4, 10 mM $MgCl_2$ supplemented with 100 nM ATP and 1 ul [$\gamma-^{32}$P]-ATP (PerkinElmer) (10 μCi) at 37°C for 30 min. The samples were subjected to SDS-PAGE followed by authoradiograph.

mRNA decay assay:

Endogenous mRNA half-lives were determined with the use of actinomycin D (5 mg/mL) to inhibit transcription. Pulse-Chase mRNA decay assay in HeLa Tet-off cells were performed as described previously [26]. Reporter RNA construct for this assay was obtained by cloning CXCL1 220 (720–940) into pTRE2 (Clontech) containing 5'UTR and coding region of CXCL1 as described previously[26] (KCΔ4). Transcription in the tet-off system is under control of a tetracycline-response element (TRE). In the absence of tetracycline or its analog doxycycline, the tetracycline transactivator drives transcription of the reporter mRNA. After the addition of doxycycline to the culture medium, transcription is abolished, which allows to measure the rate of reporter mRNA decay. We treated the transfected cells with doxycycline to allow reporter CXCL1 mRNA to decay for 0, 45 and 90 min and assessed remaining reporter CXCL1 220 mRNA and GAPDH mRNA. Total RNA was isolated by TRIzol reagent (Invitrogen) following the manufacturer's instruction, followed by RT-PCR. The values were normalized to the stable GAPDH mRNA.

Microscopy:

IHC staining was recorderd with an OLYMPUS DP71 digital camera attached to an Olympus BX41 microscope. Fluorescent images were captured with Leica confocal Microscope (Lerner Institute imaging core). As a routine practice, three independent plates of cells were analyzed for quantification with a total of 50 cells analyzed from each plate.

Statistical analyses:

Statistical analysis was applied to biologically independent samples (separate plates of cells or mice) from very single experiment and data were not pooled from independent experiments for statistical analysis. Experiments were repeated at least twice and the exact number of repetition is indicated in figure legend for each panel. For all RT-PCR and ELISA analyses, at least 3 biological replicates (separate plate of cells) were used. Unless otherwise indicated, comparison between two groups were analyzed by two-tailed Student's *t* test. All bar graphs show mean and standard deviation or standard of error, which is indicated for each panel in the figure legend. The exact P value for each comparison is provided in the graph or as p value < 0.001. Statistical analysis of mass-spectrometry and microarray data are detailed in their respective sections. GraphPad Prism 7 was used for data analysis and representation.

Supplementary Material

Refer to Web version on PubMed Central for supplementary material.

Acknowledgements

We would like to thank J. Lykke-Andersen (University of California, San Diego); V. Heissmeyer (Biomedical Center Munich) and M. Kiledjian (Rutgers University) for plasmids. This work is supported by the US National Institutes of Health (P01HL103453; P01 CA062220; P01 HL 029582), and grand from NMSS (RG5130A2/1).

References

1. Harrington LE et al. Interleukin 17–producing CD4+ effector T cells develop via a lineage distinct from the T helper type 1 and 2 lineages. Nature immunology 6, 1123 (2005).16200070
2. Park H et al. A distinct lineage of CD4 T cells regulates tissue inflammation by producing interleukin 17. Nature immunology 6, 1133 (2005).16200068
3. Cua DJ & Tato CM Innate IL-17-producing cells: the sentinels of the immune system. Nature Reviews Immunology 10, 479 (2010).
4. Kolls JK & Khader SA The role of Th17 cytokines in primary mucosal immunity. Cytokine & growth factor reviews 21, 443–448 (2010).21095154
5. Patel DD , Lee DM , Kolbinger F & Antoni C Effect of IL-17A blockade with secukinumab in autoimmune diseases. *Annals of the rheumatic diseases,* annrheumdis-2012–202371 (2012).
6. Swaidani S et al. The critical role of epithelial-derived Act1 in IL-17-and IL-25-mediated pulmonary inflammation. The Journal of Immunology 182, 1631–1640 (2009).19155512
7. Toy D et al. Cutting edge: interleukin 17 signals through a heteromeric receptor complex. The Journal of Immunology 177, 36–39 (2006).16785495
8. Shen F & Gaffen SL Structure–function relationships in the IL-17 receptor: implications for signal transduction and therapy. Cytokine 41, 92–104 (2008).18178098
9. Novatchkova M , Leibbrandt A , Werzowa J , Neubüser A & Eisenhaber F The STIR-domain superfamily in signal transduction, development and immunity. Trends in biochemical sciences 28, 226–229 (2003).12765832

10. Li X et al. Act1, an NF-κB-activating protein. Proceedings of the National Academy of Sciences 97, 10489–10493 (2000).
11. Chang SH , Park H & Dong C Act1 adaptor protein is an immediate and essential signaling component of interleukin-17 receptor. Journal of Biological Chemistry 281, 35603–35607 (2006). 17035243
12. Qian Y et al. The adaptor Act1 is required for interleukin 17–dependent signaling associated with autoimmune and inflammatory disease. Nature immunology 8, 247 (2007).17277779
13. Gu C , Wu L & Li X IL-17 family: cytokines, receptors and signaling. Cytokine 64, 477–485 (2013).24011563
14. Stoecklin G , Mayo T & Anderson P ARE-mRNA degradation requires the 5′–3′ decay pathway. EMBO reports 7, 72–77 (2006).16299471
15. Leppek K et al. Roquin promotes constitutive mRNA decay via a conserved class of stem-loop recognition motifs. Cell 153, 869–881 (2013).23663784
16. Stumpo DJ , Lai WS & Blackshear PJ Inflammation: cytokines and RNA-based regulation. Wiley Interdisciplinary Reviews: RNA 1, 60–80 (2010).
17. Schoenberg DR & Maquat LE Regulation of cytoplasmic mRNA decay. Nature Reviews Genetics 13, 246 (2012).
18. Mino T et al. Regnase-1 and roquin regulate a common element in inflammatory mRNAs by spatiotemporally distinct mechanisms. Cell 161, 1058–1073 (2015).26000482
19. Brennan CM & Steitz JA HuR and mRNA stability. Cellular and Molecular Life Sciences CMLS 58, 266–277 (2001).11289308
20. Herjan T et al. HuR is required for IL-17–induced Act1-mediated CXCL1 and CXCL5 mRNA stabilization. The Journal of Immunology 191, 640–649 (2013).23772036
21. Erickson SL & Lykke-Andersen J Cytoplasmic mRNP granules at a glance. J Cell Sci 124, 293–297 (2011).21242308
22. Anderson P , Kedersha N & Ivanov P Stress granules, P-bodies and cancer. Biochimica et Biophysica Acta (BBA)-Gene Regulatory Mechanisms 1849, 861–870 (2015).25482014
23. Velichko S et al. A novel nuclear function for the interleukin-17 signaling adaptor protein Act1. PloS one 11, e0163323 (2016).27723765
24. Liu C et al. A CC′ Loop Decoy Peptide Blocks the Interaction Between Act1 and IL-17RA to Attenuate IL-17–and IL-25–Induced Inflammation. Sci. Signal. 4, ra72–ra72 (2011).22045852
25. Hartupee J , Liu C , Novotny M , Li X & Hamilton T IL-17 enhances chemokine gene expression through mRNA stabilization. The Journal of Immunology 179, 4135–4141 (2007).17785852
26. Datta S et al. IL-17 regulates CXCL1 mRNA stability via an AUUUA/tristetraprolin-independent sequence. The journal of immunology 184, 1484–1491 (2010).20042592
27. Hartupee J et al. IL-17 signaling for mRNA stabilization does not require TNF receptor-associated factor 6. The Journal of Immunology 182, 1660–1666 (2009).19155515
28. Wang Z , Jiao X , Carr-Schmid A & Kiledjian M The hDcp2 protein is a mammalian mRNA decapping enzyme. Proceedings of the National Academy of Sciences 99, 12663–12668 (2002).
29. She M et al. Structural basis of dcp2 recognition and activation by dcp1. Molecular cell 29, 337–349 (2008).18280239
30. Rzeczkowski K et al. c-Jun N-terminal kinase phosphorylates DCP1a to control formation of P bodies. The Journal of cell biology 194, 581–596 (2011).21859862
31. Aizer A , Kafri P , Kalo A & Shav-Tal Y The P body protein Dcp1a is hyper-phosphorylated during mitosis. PloS one 8, e49783 (2013).23300942
32. Bulek K et al. The inducible kinase IKKi is required for IL-17-dependent signaling associated with neutrophilia and pulmonary inflammation. Nature immunology 12, 844 (2011).21822257
33. Qu F et al. TRAF6-dependent Act1 phosphorylation by the IκB kinase-related kinases suppresses interleukin-17-induced NF-κB activation. Molecular and cellular biology 32, 3925–3937 (2012). 22851696
34. Zhong X-Y , Wang P , Han J , Rosenfeld MG & Fu X-D SR proteins in vertical integration of gene expression from transcription to RNA processing to translation. Molecular cell 35, 1–10 (2009). 19595711

35. Bresson S , Tuck A , Staneva D & Tollervey D Nuclear RNA decay pathways aid rapid remodeling of gene expression in yeast. Molecular cell 65, 787–800. e785 (2017).28190770
36. Sun D et al. Treatment with IL-17 prolongs the half-life of chemokine CXCL1 mRNA via the adaptor TRAF5 and the splicing-regulatory factor SF2 (ASF). Nature immunology 12, 853 (2011). 21822258
37. Huynh N et al. Allosteric interactions direct binding and phosphorylation of ASF/SF2 by SRPK1. Biochemistry 48, 11432–11440 (2009).19886675
38. Tiedje C et al. The p38/MK2-driven exchange between tristetraprolin and HuR regulates AU–rich element–dependent translation. PLoS genetics 8, e1002977 (2012).23028373
39. Chesné J et al. Prime role of IL-17A in neutrophilia and airway smooth muscle contraction in a house dust mite–induced allergic asthma model. Journal of Allergy and Clinical Immunology 135, 1643–1645. e1645 (2015).25649077
40. Liu C et al. The flavonoid cyanidin blocks binding of the cytokine interleukin-17A to the IL-17RA subunit to alleviate inflammation in vivo. Sci. Signal. 10, eaaf8823 (2017).28223414
41. Ryzhakov G & Randow F SINTBAD, a novel component of innate antiviral immunity, shares a TBK1-binding domain with NAP1 and TANK. The EMBO journal 26, 3180–3190 (2007). 17568778
42. Chau T-L et al. Are the IKKs and IKK-related kinases TBK1 and IKK-ε similarly activated? Trends in biochemical sciences 33, 171–180 (2008).18353649
43. Nakatsu Y et al. Functionally distinct effects of the C-terminal regions of IKKε and TBK1 on type I IFN production. PloS one 9, e94999 (2014).24722368
44. Helgason E , Phung QT & Dueber EC Recent insights into the complexity of Tank-binding kinase 1 signaling networks: the emerging role of cellular localization in the activation and substrate specificity of TBK1. FEBS letters 587, 1230–1237 (2013).23395801
45. Ruzankina Y et al. Deletion of the developmentally essential gene ATR in adult mice leads to age-related phenotypes and stem cell loss. Cell stem cell 1, 113–126 (2007).18371340
46. Zhang B et al. Structure of the unique SEFIR domain from human interleukin 17 receptor A reveals a composite ligand-binding site containing a conserved α-helix for Act1 binding and IL-17 signaling. Acta Crystallographica Section D: Biological Crystallography 70, 1476–1483 (2014). 24816115
47. Datta S et al. Tristetraprolin regulates CXCL1 (KC) mRNA stability. The Journal of Immunology 180, 2545–2552 (2008).18250465
48. Deng J et al. An improved protocol for rapid freezing of protein samples for long-term storage. Acta Crystallographica Section D: Biological Crystallography 60, 203–204 (2004).14684931
49. Deng J et al. Structure of the ROC domain from the Parkinson's disease-associated leucine-rich repeat kinase 2 reveals a dimeric GTPase. Proceedings of the National Academy of Sciences 105, 1499–1504 (2008).

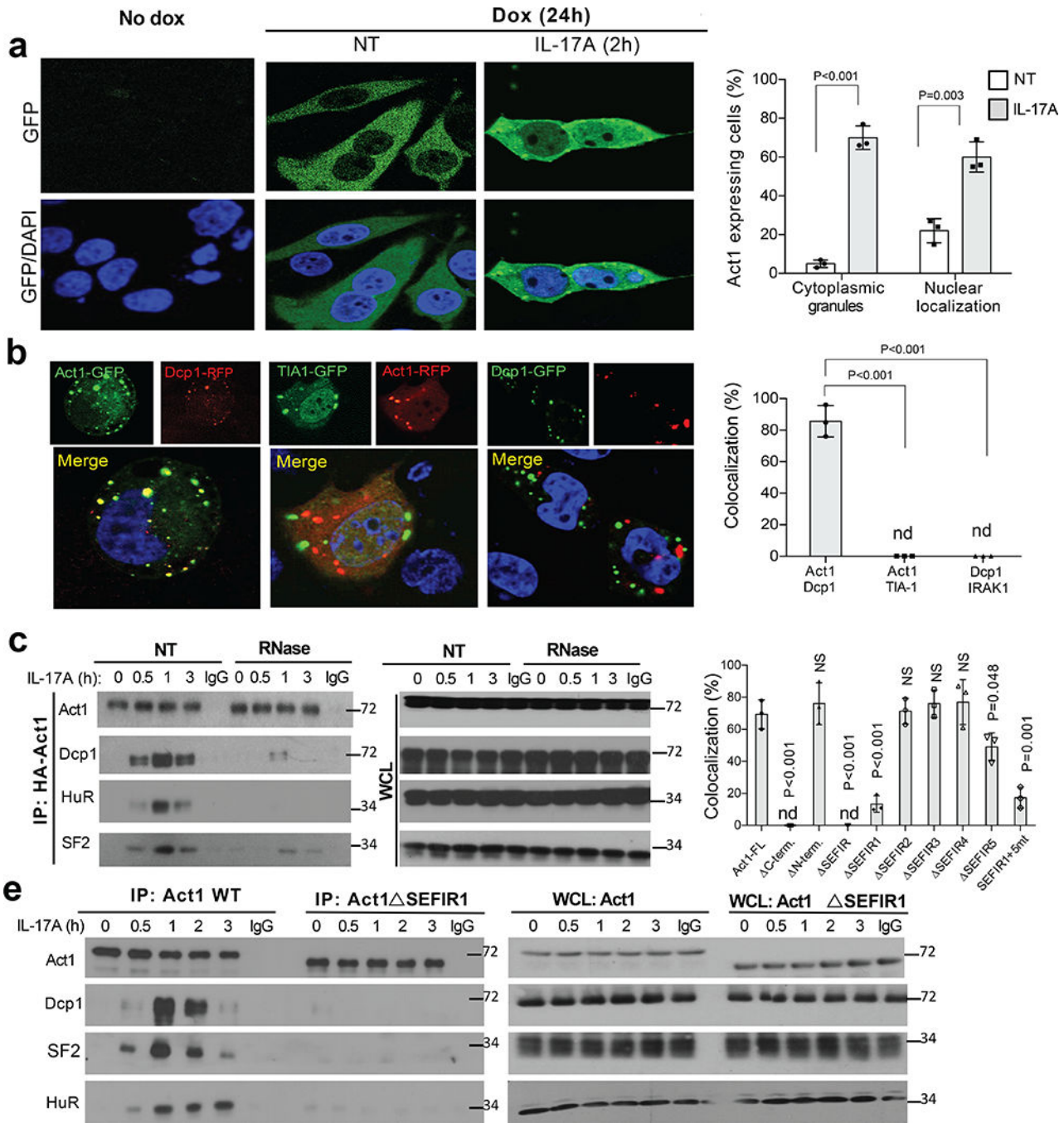

Figure 1. IL-17A induces distinct Act1-RNPs in the nucleus and cytoplasmic granules.

a. Confocal imaging of Act1-GFP in HeLa Tet-On stable cell line induced by doxycycline for 24 hours followed by IL-17A stimulation. Nuclei stained with DAPI in blue. Bar graph shows the mean and s.d. of percentages (n=3 independent plates of cells) of cells that display Act1 in the cytoplasmic granules or nuclear localization. 50 cells per plate were analyzed for quantification. **b**. Confocal imaging of HeLa cells co-transfected with GFP- or RPF-tagged expression constructs as indicated. Nuclei stained with DAPI in blue. Bar graph shows the mean and s.d. of percentages (n=3 independent plates of cells) of cells with co-localization

of the two expressing proteins [Act1/Dcp1; Act1/TIA1 and Dcp1/IRAK1(IL-1R associated kinase 1)]. 50 cells per plate were analyzed for quantification. **c.** Lysates from primary MEFs (isolated from LSL–HA–Act1 knock-in mice) stimulated with IL-17A (50 ng/ml), either left untreated or treated with RNase A, were immunoprecipitated (IP) using anti-HA (for endogenous HA-Act1) followed by Western blot analysis with the indicated antibodies. The data are representative of three independent experiments. **d.** Bar graph shows the mean and s.d. (n=3 independent plates of cells) of percentages of cells with co-localization of Dcp1 with full-length Act1 or Act1 deletion mutants (Supplemental. Fig. 1g). 50 expressing cells per plate were analyzed for quantification. **e**. $Act1^{-/-}$ MEFs reconstituted by retroviral infection with either FLAG-tagged mouse wild-type Act1 (WT) or SEFIR1 deletion mutant were treated with IL-17A (50 ng/ml). The cell lysates were immunoprecipitated (IP) with anti-FLAG followed by Western blot analysis using antibodies as indicated. All data are representative of two independent experiments. The exact P value for each comparison is provided on the graph or as p value < 0.001. Scale bars, 20 μm.

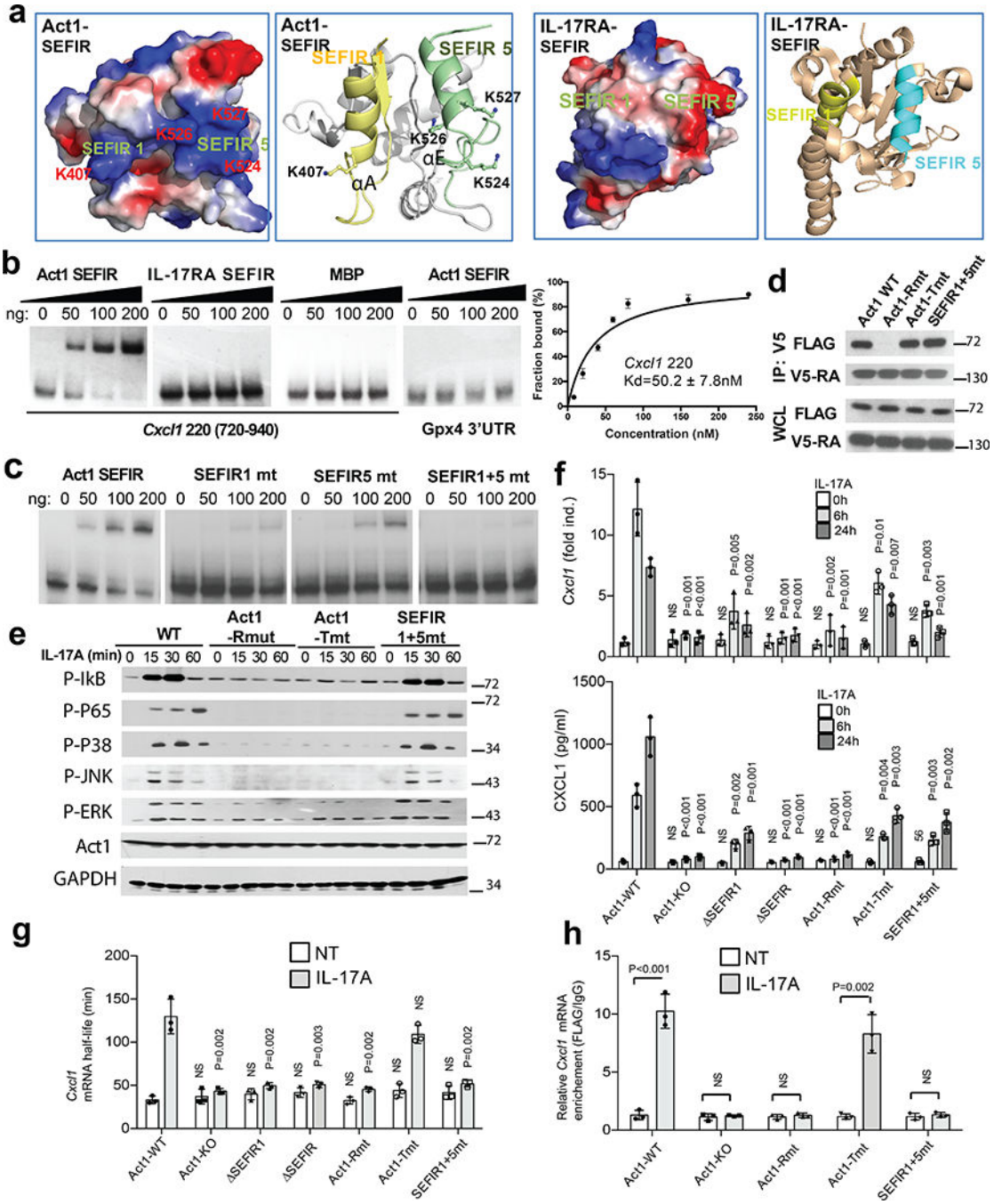

Figure 2. Act1 directly binds to the CXCL1 3'UTR through the SEFIR domain

a. The structure model of Act1-SEFIR. Blue and Red: positive and negative electrostatic potential. **b.** Binding of purified recombinant Act1 SEFIR, IL-17RA SEFIR and His-MBP to the *Cxcl1* 3'UTR and Gpx4 3'UTR by REMSA. Graph indicates the apparent Kd of *Cxcl1* 3'UTR (*Cxcl1* 220 as shown in Fig. 3a). Graph shows mean and s.d. **c**. REMSA of purified recombinant Act1 SEFIR and SEFIR point mutants to the *Cxcl1* 3'UTR (*Cxcl1* 220). **d.** FLAG-tagged Act1 WT and Act1 mutants were transfected into MEFs with V5-tagged IL-17RA. The cell lysates were immunoprecipated (IP) using anti-V5 followed by Western

blot analyses using the indicated antibodies. **e**. *Act1*$^{-/-}$ MEFs transfected with Act1 wild-type (Act1-WT) and Act1 mutants were treated with IL-17A for the indicated times. The cell lysates were analyzed by Western blotting with the indicated antibodies. **f.** *Act1*$^{-/-}$ MEFs transfected with vector (Act1-KO), Act1 wild-type (Act1-WT) and Act1 mutants pretreated with TNF for 1 hour, either left untreated or stimulated with IL-17A. The mRNA and protein levels were analyzed by RT-PCR (Top) and Elisa (Bottom), respectively (n=3 independent plates of cells). **g.** *Act1*$^{-/-}$ MEFs transfected with vector (Act1-KO), Act1 wild-type (Act1-WT) and Act1 mutants were pre-treated with TNF for 1 hour and then treated with Actinomycin D alone (NT) or in the presence of IL-17A for 25, 50, 70, and 100min, followed by RT-PCR analysis (n=3 independent plates of cells). The indicated mRNA levels were normalized to GAPDH and presented as half-life. **h**. *Act1*$^{-/-}$ MEFs transfected with vector (Act1-KO), flag-tagged Act1 wild-type (Act1-WT) and Act1 mutants were pre-treated with TNF for 1 hour and then treated with IL-17A for 0 and 60 min followed by RNA immunoprecipitation with anti-FLAG and RT-PCR analyses of the indicated mRNAs (n=3 independent plates of cells). The presented are the relative values to levels from IgG immunoprecipitation. Bar graph shows mean and s.d. of independent plates of cells (**f-h**). The exact P value for each comparison (Act1-WT versus Act1 mutants) is provided in the graph or as p value < 0.001. Data are representative of two (panels **c-h**) or three (panel **b**) independent experiments.

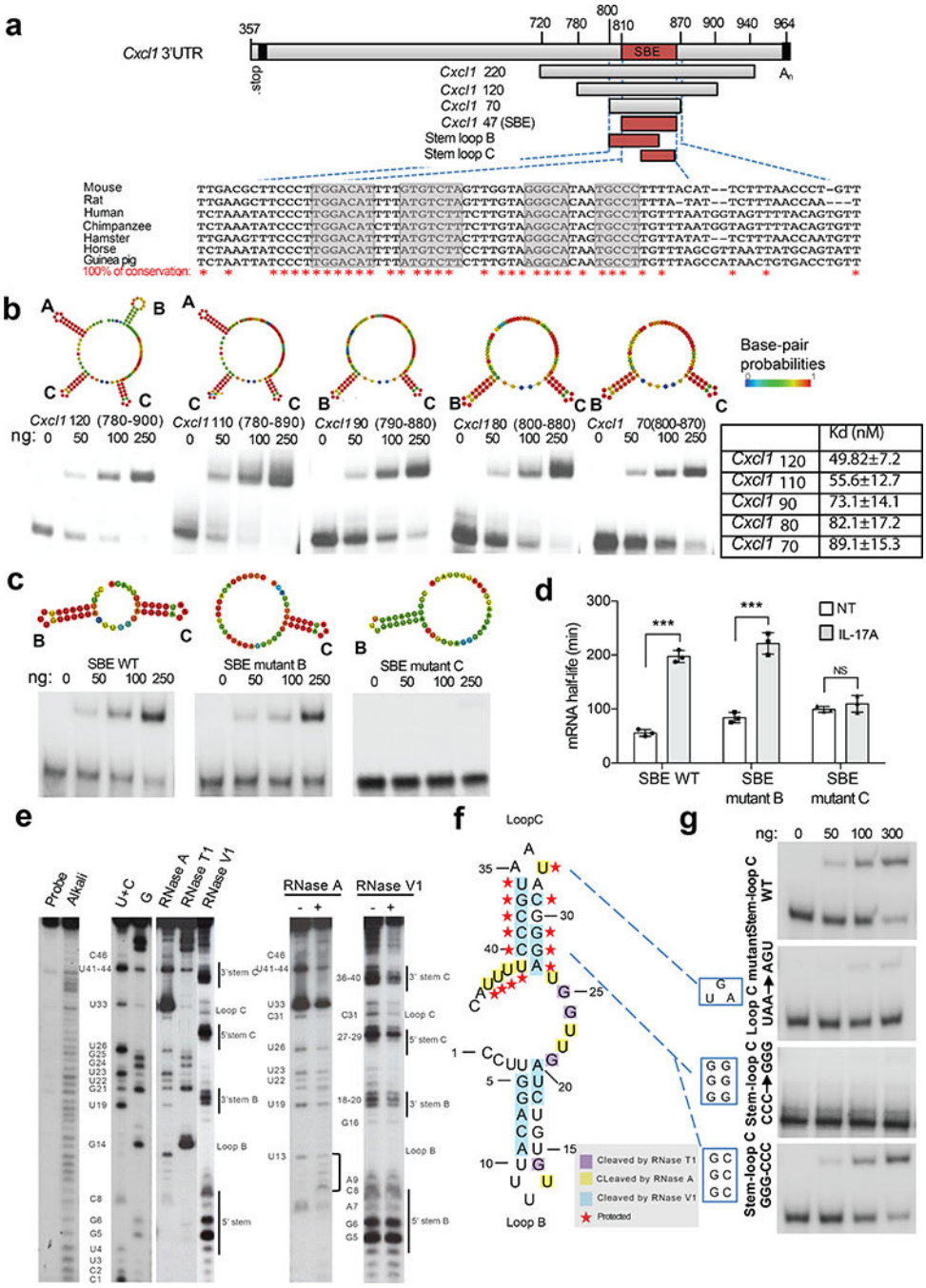

Figure 3. Act1 SEFIR binds to a stem-loop structure in *Cxcl1* 3'UTR.

a. Schematic representation of the mouse *Cxcl1* 3'UTR together with an alignment of the region containing conserved stem-loops in the *Cxcl1* 3'UTRs from indicated species. Shaded boxes: conserved stem-loops. **b**. REMSA for the binding of purified recombinant Act1 SEFIR to the serial deletion mutants from both ends of *Cxcl1* 220 (shown in **a**). Table shows the apparent Kds of the serial deletion mutants. **c**. Binding of purified recombinant Act1 SEFIR to SEFIR Binding Element (SBE WT, *Cxcl1* 47 as indicated in **a**) and stem-loop B and stem-loop C disruption mutants. **d**. Real-time PCR analysis (n=3 independent

plates of cells) of *Cxcl1* mRNA in HeLa Tet-Off cells transfected with pTRE2 [26] with and without stem-loop B or stem-loop C disruption mutation, treated with doxycycline alone or together with IL-17A for 0, 45 or 90 min. *Cxcl1* mRNA levels were normalized to GAPDH and presented as half-life**e**. The 5' end-labeled *Cxcl1* SBE was incubated in the absence or presence of Act1 SEFIR. The reactions were then partially digested with RNase T1, A, or V1 as indicated. The sequencing (G and C + U) and alkali ladders are shown in the left lanes. The numbers to the left of the gel indicate the positions of nucleotides using the numbering in (**f**). The bands above C46 are resulted from the remaining sequence in plasmid template after restriction enzyme cutting. The different regions of the SBE are indicated. The red boxes indicate protected nucleotides in the SBE that were consistently observed. **f**. The structure of the SEFIR binding element from the mouse *Cxcl1* mRNA is shown. Stars indicate nucleotides that are protected from cleavage by RNase A and V1. **g.** Binding of purified recombinant Act1 SEFIR to the Stem-loop C and mutants were examined by REMSA. Bar graph shows mean and s.d. of independent plates of cells (**d**). The exact P value for each comparison is provided in the graph or as p value < 0.001. Data are representative of 2 (panel **c**) or 3 (panel **b, d-e** and **g**) independent experiments.

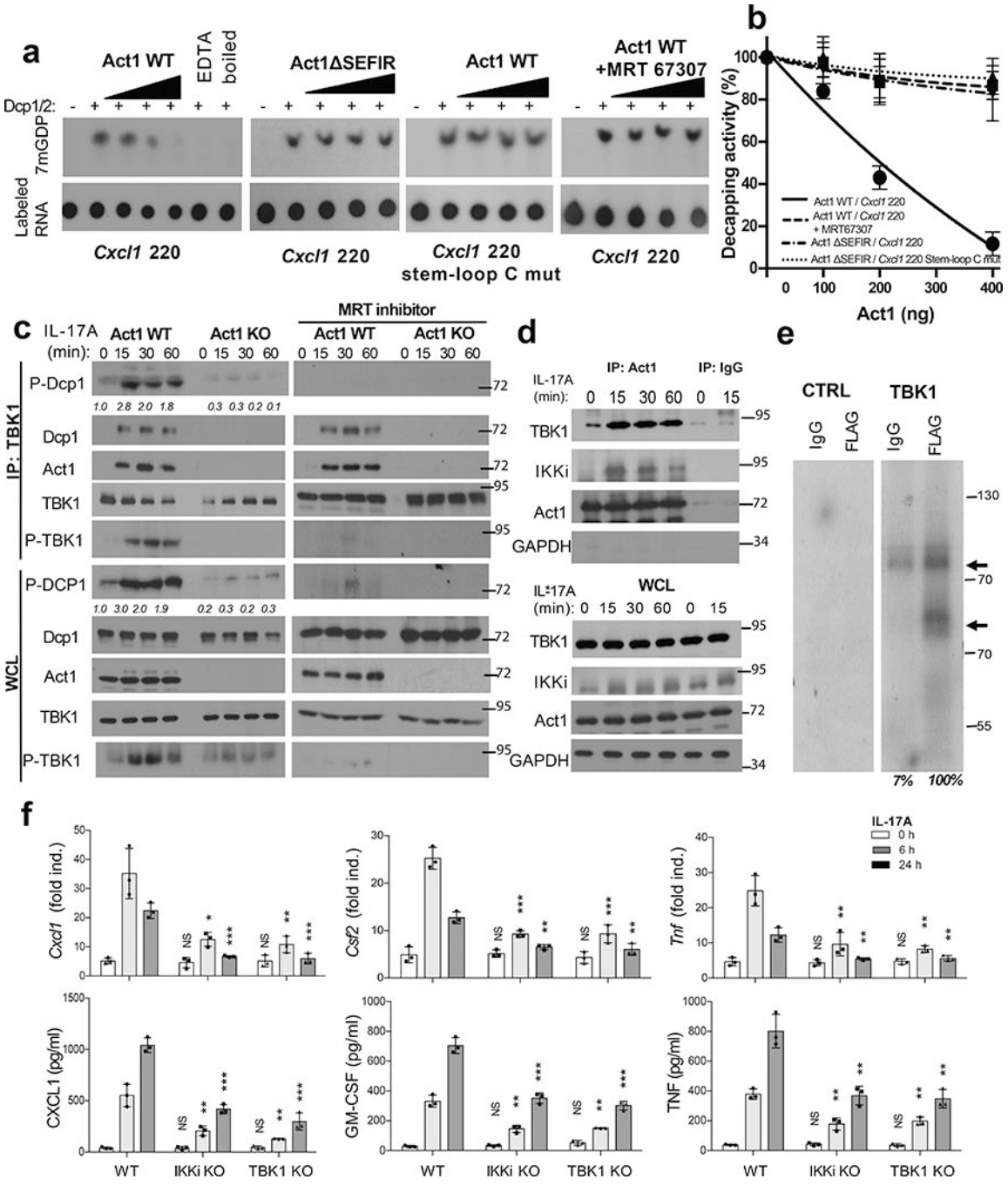

Figure 4. Act1-RNA binding to 3'UTR inhibits decapping through TBK1-mediated phosphorylation of Dcp1.

a. Cap (m7GDP) labeled reporter RNAs [*Cxcl* 220 and mutant without stem-loop C (*Cxcl* 220-stem-loop C mutant)] were subjected to decapping assay using purified Dcp1/Dcp2 with increasing amounts of purified Act1 WT or Act1 ΔSEFIR in the presence or absence of TBK1 inhibitor (MRT67307). EDTA and boiling were included as negative controls to inactivate Dcp1/Dcp2 enzymatic activity. Radiograms were quantified by densitometry. **b.** Graph indicates the decapping activity calculated by quantifying the released Cap as a

percentage of the amount of Cap catalyzed by purified Dcp1/2. **c.** Cell lysates from *Act1*$^{-/-}$ MEFs with and without reconstitution of wild-type Act1 (Act1-WT and Act1-KO) with or without the presence of TBK1 inhibitor (MRT67307) were immunoprecipitated (IP) with anti-TBK1 followed by Western blot analysis using antibodies as indicated. **d.** Cell lysates from untreated and IL-17A-treated HeLa cells were immunoprecipitated (IP) with anti-Act1 followed by Western blot analysis using antibodies as indicated. **e.** *In vitro* kinase assay of Dcp1 by recombinant TBK1 using Dcp1-immunoprecipitates from HeLa cells transfected with FLAG-tagged Dcp1. **f.** Wild-type (WT), IKKi-deficient (IKKi KO) and TBK1-deficient (TBK1 KO) MEFs pretreated with TNF for 1 hour, were untreated or stimulated with IL-17A. The mRNA and protein levels were then analyzed by RT-PCR (Top) and Elisa (Bottom), respectively (n=3 independent plates of cells). Bar graph shows mean and s.d. of independent plates of cells (f). The exact P value for each comparison is provided in the graph or as p value < 0.001. Data are representative of two (panel c, d, f) or three (panel a, e) independent experiments.

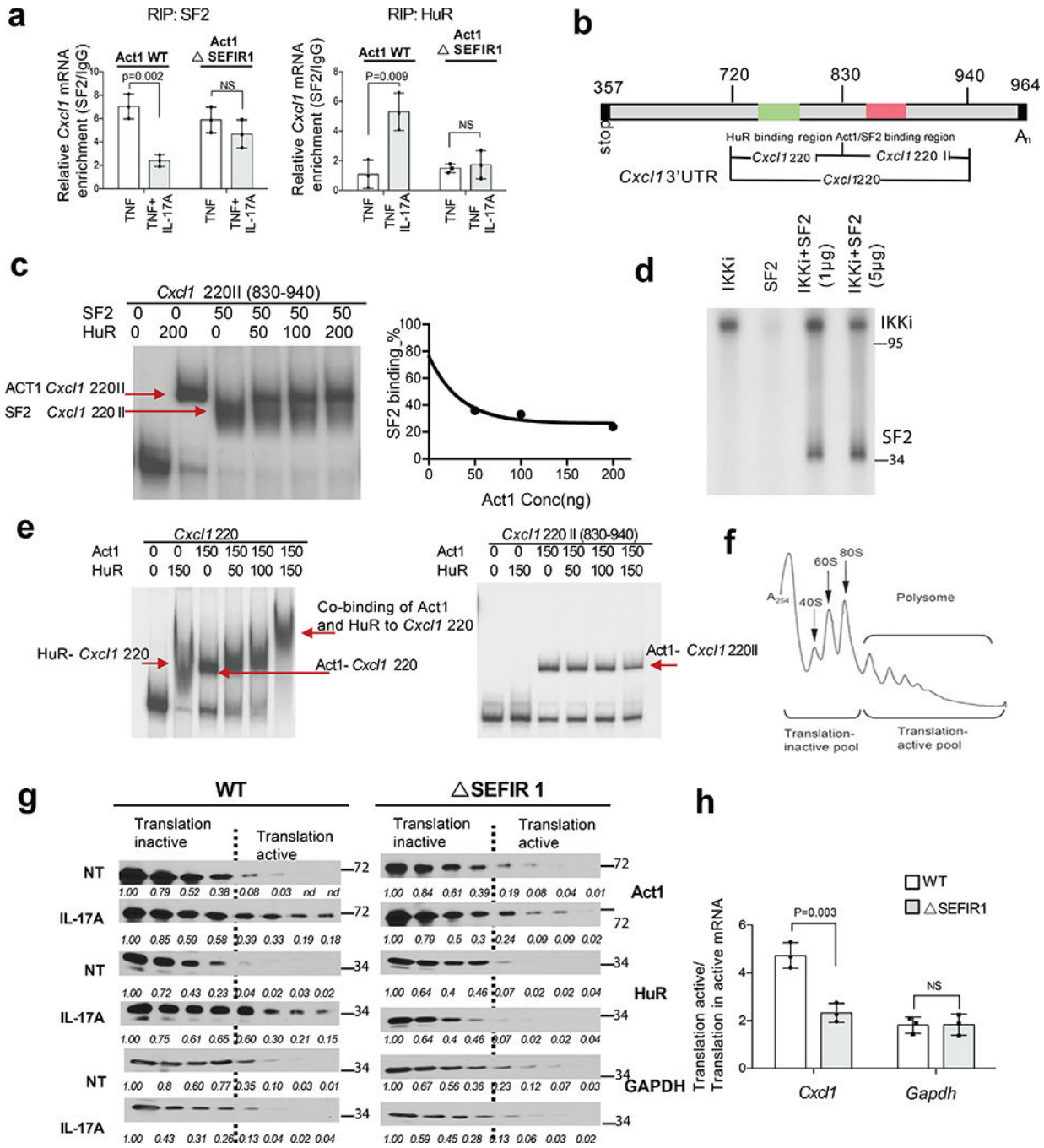

Figure 5. Act1 forms distinct RNPs with Dcp1, Dcp2, SF2 and HuR.

a. *Act1*$^{-/-}$ MEFs reconstituted by retroviral infection with either wild-type Act1 (WT) or ΔSEFIR1 were pre-treated with TNF for 1 hour and then treated with IL-17A for 0 and 60 min followed by RNA immunoprecipitation with anti-SF2 or anti-HuR, and RT-PCR analyses (n=3 independent plates of cells) of the indicated mRNAs. The presented are the relative values normalized against IgG control. **b.** Schematic representation of the mouse CXCL1 3'UTR. HuR, Act1 and SF2 binding regions are indicated. **c**. Act1-SEFIR and SF2 RNA binding competition was performed using probe *Cxcl1* 220 II (as indicated in **b)**.

Graph indicates the dissociation of SF2-*Cxcl1* 220 II upon incubation with increasing amounts of Act1-SEFIR, which was calculated by quantifying the remaining SF2-*Cxcl1* 220 II complex in the presence of indicated amounts of Act1-SEFIR. **d.** In vitro kinase assay of purified recombinant IKKi using purified recombinant SF2 as a substrate. **e.** The simultaneous binding of purified recombinant HuR and Act1-SEFIR to *Cxcl1* 3'UTR was examined by REMSA using *Cxcl1* 220 and *Cxcl1* 220 II as probes. The co-binding Act1-HuR was observed with probe *Cxcl1*-220, but not *Cxcl1*-220 II. **f.** UV-absorbance profile of RNP and polysome complexes separated on a sucrose density gradient into different fractions as indicated. **g.** Cytoplasmic extracts of $Act1^{-/-}$ MEFs reconstituted by retroviral infection with either FLAG-tagged mouse wild-type Act1 (WT) or SEFIR1 deletion mutant, pre-treated with TNF for 1 hour and then treated with IL-17A for 0 and 90 min, were fractionated through a 10–50% sucrose gradient and analyzed by Western blot analyses with the indicated antibodies. **h.** *Cxcl1* mRNAs from translation-active pools and translation-inactive pools from **f** were analyzed by RT-PCR and normalized to β-actin. Graph shows the ratios of mRNAs from translation-active/inactive pools (n=3 independent plates of cells). All data are representative of three independent experiments. Bar graph shows mean and s.d. of independent plates of cells (**a, h**). The exact P value for each comparison is provided in the graph or as p value < 0.001.

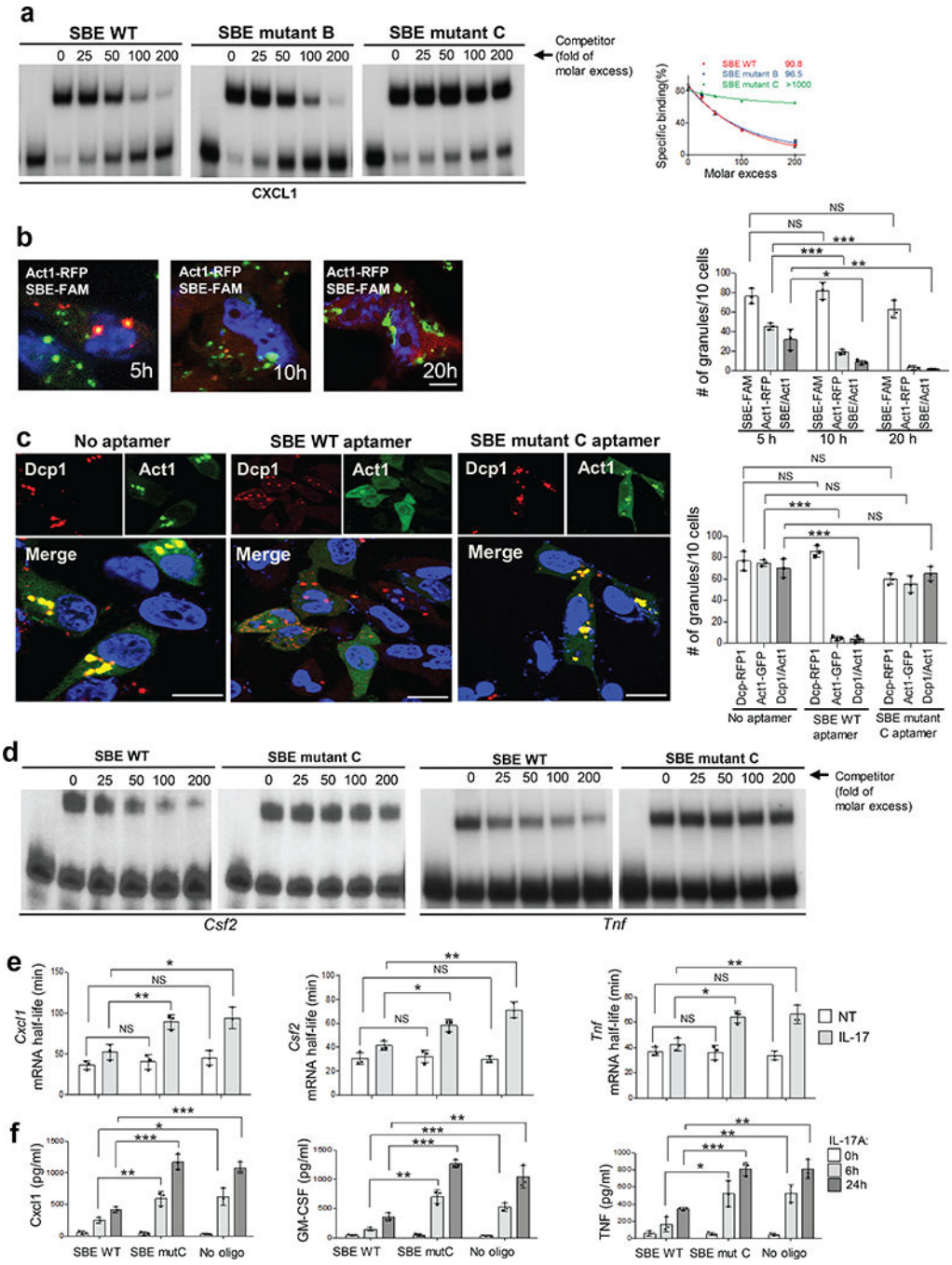

Figure 6.

Model of Act1-RNP in mRNA stabilization: Act1 directly binds to the mRNAs of inflammatory genes to form multiple RNPs controlling different steps of mRNA metabolism in response to IL-17A stimulation. Upon IL-17A stimulation, Act1 is translocated into the nucleus where Act1 binds to a stem-loop structure in the 3'UTR in the target mRNAs (RNP1). The binding of Act1 competes off SF2 from the mRNAs by bringing IKKi to phosphorylate SF2, preventing SF2-mediated mRNA decay. Act1 then follows the mRNAs to the P-bodies (RNP2) inhibiting Dcp1/2-mediated mRNA decapping by employing TBK1

to phosphorylate Dcp1. Finally, Act1-mRNAs are shifted to the polysomes to facilitate HuR's binding to mRNAs (RNP3) for protein translation.

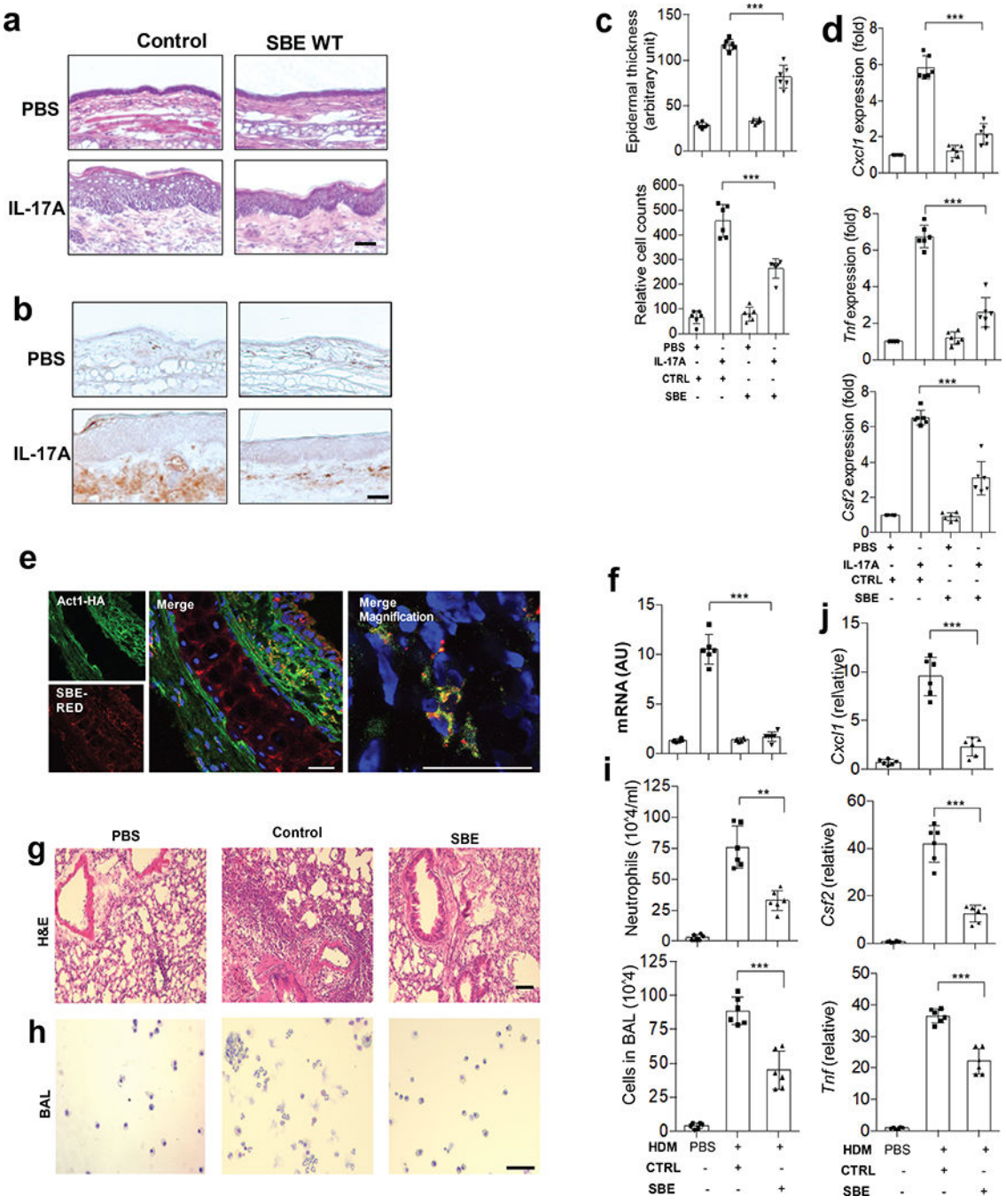

Figure 7. SBE RNA aptamers abolished IL-17A-induced mRNA stabilization of *Cxcl1*, *Csf2* and *Tnf*.

a. SBE RNA aptamers [SBE WT (*Cxcl1* 47), SBE mutant B and SBE mutant C] were used to compete with *Cxcl1* 220 probe for binding to Act1-SEFIR. Graph quantifies the remaining Act1-SEFIR-bound *Cxcl1* 220 probe in the presence of indicated concentrations of SBE aptamers. **b**. Confocal imaging of RFP-Act1 and fluorescein amidite labeled SBE aptamer (SBE-FAM) in transfected HeLa cells. Nuclei were stained with DAPI in blue. Graph indicates the average numbers and s.d. (n=3 independent plates of cells) of SBE-

FAM-positive, Act1-RFP-positive and SBE-FAM/Act1-RFP-double positive granules per 10 cells at 5, 10 and 20 hours after SBE-FAM transfection. 50 cells per plate were analyzed for quantification. **c**. Confocal imaging of Dcp1-RFP and Act1-GFP expressing HeLa cells transfected with 100 pmoles/ml of unlabeled SBE aptamers. Nuclei were stained with DAPI in blue. Graph indicates the average numbers and s.d. (n=3 independent plates of cells) of Dcp1-RFP-positive, Act1-GFP-positive and Dcp1-RFP/Act1-GFP-double positive granules per 10 cells 24 hours after SBE-FAM transfection. 50 cells per plate were analyzed for quantification. **d**. SBE RNA aptamers [SBE WT (*Cxcl1* 47) and SBE mutant C] were used to compete with GM-CSF 3'UTR (513–785) and TNF 3'UTR (1362–1507) probes for binding to Act1-SEFIR. **e**. RNA decay in HeLa cells transfected with or without 100 pmoles/ml of SBE RNA aptamers (WT or mutant C), pre-treated with TNF for 1 hour and then treated with Actinomycin D alone (NT) or in the presence of IL-17A for 45 and 90 minutes. Human *Cxcl1*, *Csf2* and *Tnf* mRNAs were measured by RT-PCR (n=3 independent plates of cells), normalized to GAPDH and presented as half-life. **f.** HeLa cells transfected with or without 100 pmoles/ml of SBE RNA aptamers (WT or mutant C) were pre-treated with TNF (10 ng/ml) for 1 hour followed by stimulation with IL-17A for 0, 6 or 24 hours. Supernatants of the treated cells were then analyzed by ELISA. Data are representative of two (panel **a, d**) or three (panel **b, c, e and f**) independent experiments. Bar graph shows mean and s.d. of independent plates of cells. The exact P value for each comparison is provided in the graph or as p value < 0.001. Scale bars, 20 μm.